

Tectonic geomorphology of the Ottawa-Bonnechere Graben, Eastern Canada: implications for regional uplift and intraplate seismicity

Ugi K. Gusti ^{a,b}, Alexander L. Peace ^a, and Jeremy Rimando ^a

^aSchool of Earth, Environment and Society, McMaster University, Hamilton, ON, Canada; ^bGeological Engineering Study Program, Faculty of Engineering, University of Sriwijaya, Palembang, Indonesia

Corresponding author: Ugi K. Gusti (emails: gustiu@mcmaster.ca, ugikurnia@unsri.ac.id)

Abstract

In intraplate areas where regional tectonic strain is accommodated by the reactivation of pre-existing structures, the level of seismic hazard associated with faults may be underestimated due to the poor surface expression of faults, scattered earthquake distribution, and long earthquake recurrence intervals. The cause(s) of seismicity in eastern Canada remains unresolved. This is partially because surface expressions of faults have been eroded during glacial and deglacial periods and in the Ottawa-Bonnechere Graben (OBG) are undetectable until a seismic event. Morphotectonic analysis has been widely applied to assess relative tectonic activity in various geological settings. To establish whether active uplift is occurring and to investigate the spatial distribution of relative uplift rates, 131 bedrock drainage basins in OBG were analysed. The aim of this was to (1) test the applicability of geomorphic indices for quantifying active deformation, (2) quantify the spatiotemporal distribution of relative uplift rates, and (3) explore the implications for faulting mechanisms, deformation styles, and ultimately regional seismic hazard. We measured valley floor width-to-height ratio (V_f), basin elongation ratio (R_e), basin hypsometric integral, and normalized channel steepness index (k_{sn}). The results show that high relative uplift rates exist in all the six bedrock escarpment sections investigated, suggesting that they are presumably related with regional broad wavelength uplift (epeirogeny) caused by a complex interaction between far-field tectonic stress and glacial isostatic adjustment (GIA). Our analysis showed that V_f , R_e , and k_{sn} reveals no considerable spatial differences in high relative uplift rates, consistent with the Canadian Base Network GPS uplift rates.

Highlights

- Geomorphic indices are applied in a low relief and low-medium seismicity area.
- Geomorphic indices reveal a broad wavelength regional uplift and show relative tectonic activity in the OBG.
- Relatively high geomorphic indices values provide longer term deformation history compared to global positioning system (GPS) records.
- Landscape formation and river incision is driven by a complex interaction between GIA and far-field tectonic stresses.
- Relative uplift rate results show similar patterns to published GPS uplift rates.
- Possible link between relative tectonic activity and current seismicity.

Key words: Ottawa-Bonnechere Graben, western Quebec seismic zone, morphotectonic analysis, intraplate seismicity, regional uplift, Canada

1. Introduction

Eastern Canada is characterized as a stable continental region (SCR) which has a relatively lower seismicity rate and longer earthquake recurrence intervals compared to active plate tectonic zones/boundaries (Calais et al. 2016; Mazzotti and Gueydan 2018). However, strain localization resulting in seismicity is not uncommon in such intraplate continental domains (Mathew et al. 2016a; Jobe et al. 2020; Rimando et al. 2021). Gaining a better understanding of the causes of seis-

micity in SCRs, as well as the nature of intraplate seismicity, and strain rates, is of major concern in eastern North America, since many densely populated cities such as Montreal, Ottawa, and Toronto are located in this region. Although located far from a plate boundary, the SCR of eastern Canada regularly experiences seismic events of $\sim M5-6$ and, occasionally greater (Bent 1996a; Jobe et al. 2020). Eastern Canada is one such seismically active continental intraplate region which has a low strain and a low seismicity rate (Hurd and

Zoback 2012; Calais et al. 2016; Pinet et al. 2021). In addition, seismicity in eastern Canada is dominated by reactivation of inherited structures, which includes paleo-plate boundaries (Kumarapeli 1978; Lamontagne and Ranalli 1996; Rimando and Benn 2005; Rimando and Peace 2021). The number of seismic hazard studies in this region is steadily increasing partially due to rising awareness of the impact of earthquakes on the built environment (NRCC 2010; Adams 2011; Yu et al. 2016; Goda 2019a; Jobe et al. 2022).

The western Quebec seismic zone (WQSZ) is one of the seismically active areas in eastern Canada, which includes the Ottawa-Bonnechere Graben's (OBG) paleo-rift structures (Fig. 1). Morphotectonic analysis can be used to better define relative tectonic activity (Bull and McFadden 1977; Yildirim 2014). A strong relationship between high relative uplift rates and evidence of recent seismicity has been shown in other intraplate tectonic settings with low-to-moderate rates of seismic activity (Ntokos et al. 2016; Mathew et al. 2016a). For instance, in Borneo, most drainage basin geomorphic indices suggested high relative uplift rates, consistent with pre-existing structures that were categorized independently as active (Mathew et al. 2016a, b). In the WQSZ, previous neotectonic studies have mostly focused on seismology and sedimentology and less so on the earthquake geology and tectonic geomorphology (Baird et al. 2010; Bent et al. 2015; Brooks and Adams 2020; Doughty et al. 2010a, b; Ma and Motazedian 2012; Mohajer et al. 1992; Alinia et al. 2017). Additionally, there is an ongoing debate regarding the causes of Quaternary faulting, revolving around whether active deformation is due to glacial isostatic adjustment (GIA), tectonic stress-related deformation, or some combination of these two mechanisms (Adams 1989; Wallach et al. 1995).

This work represents the first quantitative morphotectonic analysis carried out to assess relative rates of uplift in the OBG. This analysis is important as it helps to constrain the role of regional deformation on the spatial distribution of uplift rates in the OBG area. For example, in the Timiskaming Graben, knickpoint analysis successfully identified several knickpoints coincident with previously mapped faults and lineaments (Bucci and Schoenbohm 2022), demonstrating the power of such morphotectonic approaches. Our study analysed watersheds along the bedrock escarpments of the OBG. These escarpments constitute the footwall of present-day reverse faults which are interpreted to result from the reactivation of pre-existing normal fault structures under the current tectonic stress field (Rimando and Peace 2021) (Fig. 1).

As such, the primary goals of this study are to (1) test the applicability of geomorphic indices for quantifying active deformation in this particular tectonic setting, which has a low relief and long earthquake recurrence intervals, (2) quantify the spatiotemporal distribution of relative uplift rates in the OBG, (3) explore the implications for fault mechanisms, deformation style, and ultimately regional seismic hazards, and (4) to determine priority sites for future detailed seismic hazard studies. We examined which indices may be related to unrecognized recently active structures or regions of active uplift. This was achieved by integrating four different geomorphic indices to characterize the spatial distribution of

relative uplift rates in this setting which is characterized by low-to-moderate seismicity and relief.

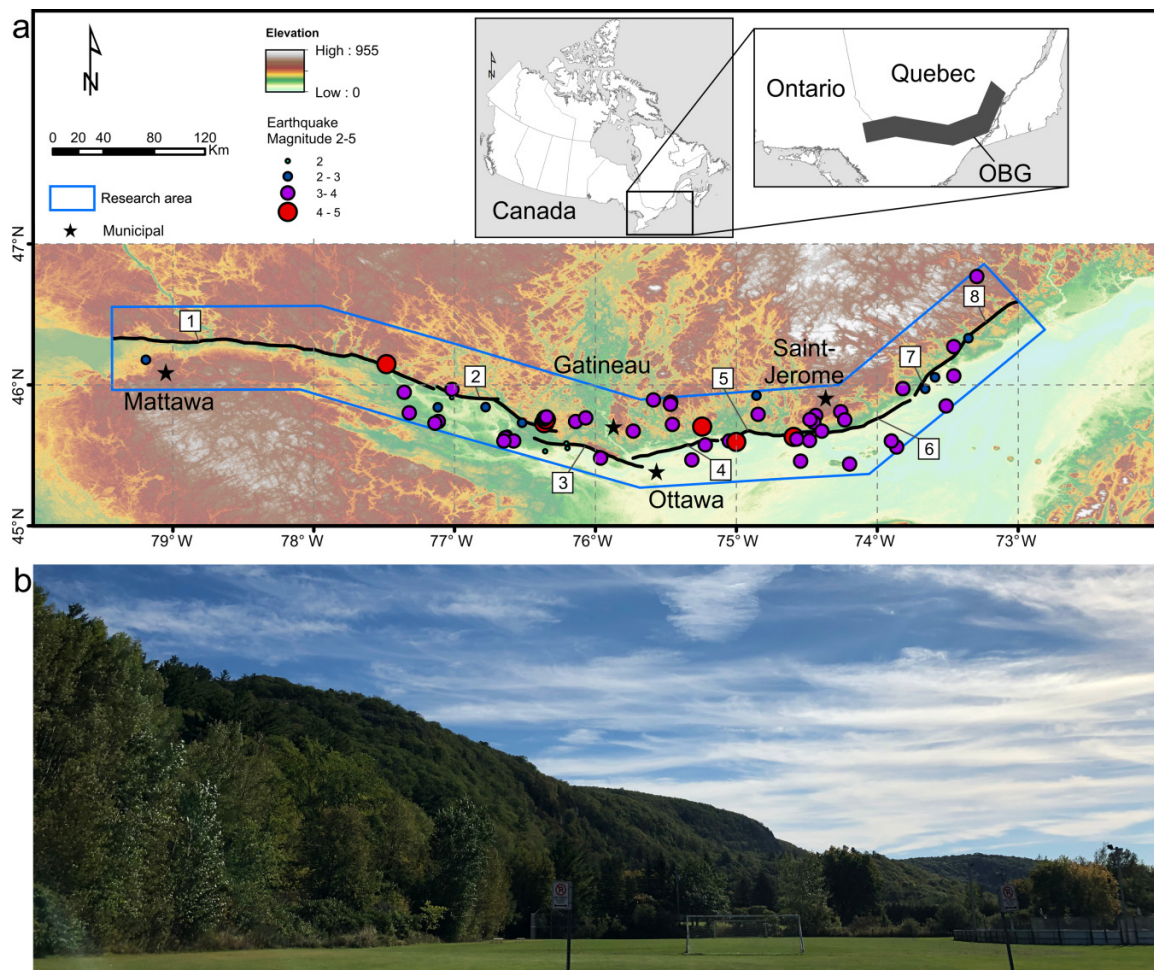
2. Regional geology

The study area is approximately 600 km wide from North Bay in the west to Montreal in the east (Fig. 1). The OBG is a part of the Saint Lawrence failed rift segment that has a complex tectonic history spanning several billion years (Lamontagne et al. 2003; Tremblay et al. 2003; Tarayoun et al. 2018). The Grenville orogeny, which started around ~1.3–1 Gyr when Laurentia and Amazonia collided shaped the early evolution of the region (Karlstrom et al. 2001; Dickin et al. 2017). The Saint Lawrence rift has two failed rift arms: (1) Ottawa-Bonnechere Graben and (2) Saguenay Graben, both of which are products of the opening of the Iapetus Ocean that took place around ~700 Myr ago (Rankin 1976). Approximately 450 Myr ago during the early stages of the Appalachian orogeny, graben development ceased with the closure of the Iapetus Ocean (Lemieux et al. 2003; Hatcher 2010). The Mesozoic–Cenozoic opening of the Atlantic Ocean represents the most recent major tectonic event that contributes to the current regional stress field (Stephenson et al. 2020). Rifting prior to the North–Central Atlantic Ocean opening was diachronous and began earlier in the Central Atlantic before rifting propagated into the North Atlantic ~150 Myr ago whereby it reactivated the paleo-rift margin of Iapetus Ocean (Lemieux et al. 2003; Tremblay et al. 2003; Peace et al. 2020; Schiffer et al. 2020). During the opening of the North Atlantic Ocean, deformation of intraplate regions likely occurred during distinct phases, which have been linked to periods of tectonic reorganisation (Stephenson et al. 2020).

The seismicity in this region is divided into seven main zones based on regional stress fields and regions of crustal weakness: (1) eastern northern Ontario, (2) southern Great Lakes, (3) western Quebec, (4) Charlevoix–Kamouraska, (5) Lower St. Lawrence, (6) northern Appalachians, and (7) Laurentian Slope seismic zones (Adams and Basham 1989; Mazzotti and Townend 2010) (Fig. 2), while, some work suggests that because the seismicity is better categorized as a single seismogenic region (Adams and Basham 1989; Vasudevan et al. 2010; Steffen et al. 2012). The band of seismicity in the WQSZ is linked to the present-day stress regime which reactivates the pre-Tertiary structures, mainly in a reverse kinematic sense with a minor strike-slip component (Figs. 1 and 2) (Wallach et al. 1995; Rimando and Benn 2005; Rimando and Peace 2021).

The OBG is tectonically part of the Grenville Province (Guo and Dickin 1996; Dickin and Guo 2001), where Precambrian rocks have experienced low rates of tectonic activity for more than 600 Myr (Fig. 2) (Guo and Dickin 1996, 2001; Rimando and Benn 2005; Ma and Eaton 2007). Seismicity in the OBG is primarily focused in the northern side and in the graben structures itself, in which reactivation of inherited structures strongly controls the seismicity distribution (Tarayoun et al. 2018), with the northwest–southeast structures playing an imperative role in the recent seismicity distribution (Rimando and Benn 2005; Rimando and Peace 2021).

Fig. 1. (a) Map of the Ottawa-Bonnechere Graben at the boundary between Quebec and Ontario Province. Major fault features (extracted from Lamontagne et al. 2003) and seismicity with earthquake magnitude from 2 to 5 (red dots = M4–5, purple dots = M3–4) (International Seismological Centre 2021) in the OBG plotted on a 30 m ASTER global digital elevation model (<https://doi.org/10.5067/ASTER/ASTGTM.003>). The blue semiparallel east–west polygon indicates the location of Fig. 5. Numbers in white boxes represent faults investigated in this study: 1, Mattawa River Fault; 2, Coulange Fault; 3, Eardley Fault; 4, Gatineau Fault; 5, Lachute fault; 6, New-Glasgow Fault; 7, Sainte-Julienne Fault; 8, Saint-Maurice Fault. (b) Photograph looking to the northeast showing the typical morphology of a northwest–southeast-oriented bedrock escarpment (goalpost as a scale approximately 2.5 m).



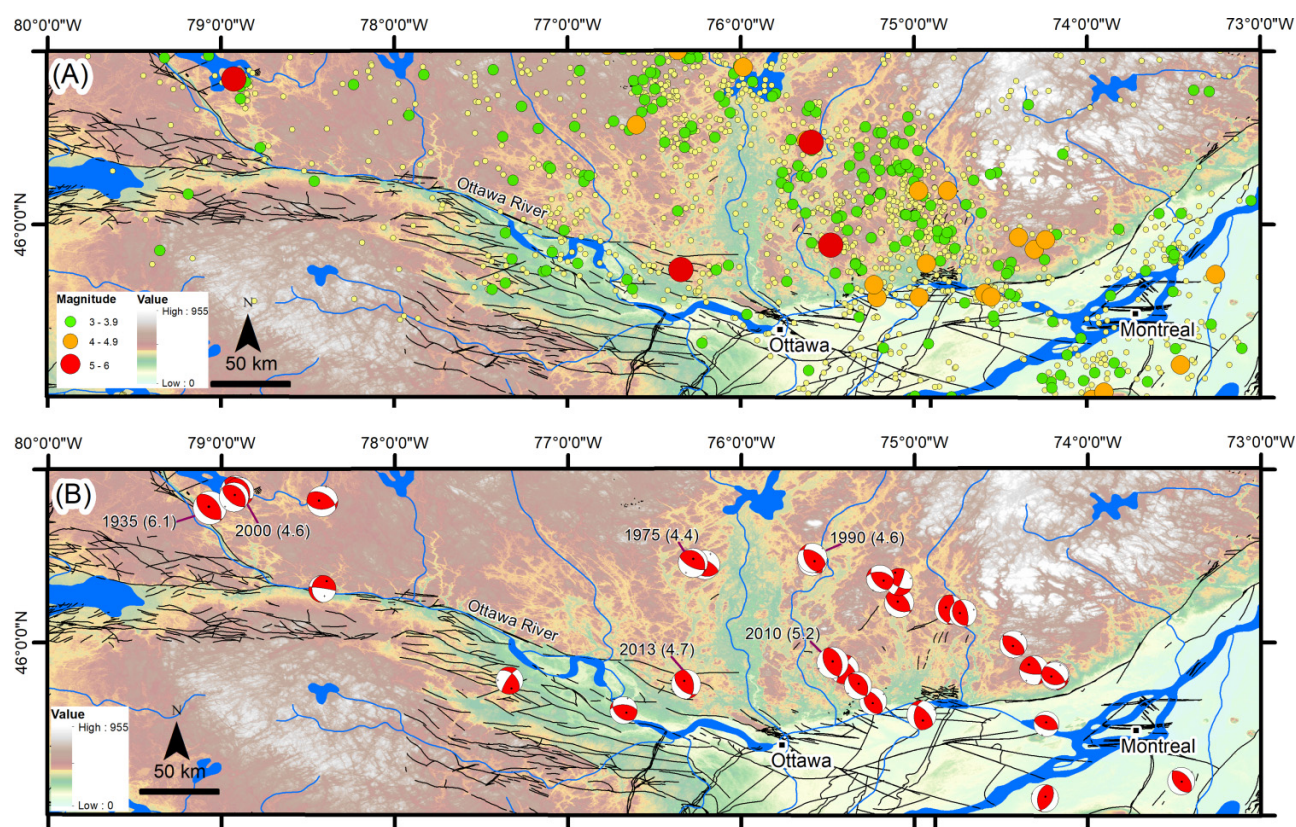
The dominating lithologies in the OBG are metamorphic rocks, predominantly Mesoproterozoic gneisses (Mezger et al. 1993) (Fig. 3). The Geological Map of Canada Map D1860 A (Wheeler et al. 1996) shows metamorphic rocks in the western and central parts of the studied area, while the sedimentary rocks dominate the eastern section. Palaeozoic sedimentary strata with an age of 453.36 ± 0.38 Ma (upper Ordovician) (Oruche et al. 2018) occupy lowland regions that overlap with the St. Lawrence lowland. The surficial deposits of the OBG consist of glacial, fluvial, and marine sediments (Brooks 2013) that date back 10 000–12 000 years (Russell et al. 2011).

3. Methodology and data

Morphotectonics is a branch of geomorphology that studies the Earth's surface relief features and relates them to tec-

tonic processes (Kober 1928). Morphotectonic analysis which integrates multiple geomorphic indices, has been used successfully to identify the relative tectonic uplift rate associated with the present-day seismicity and regional stress in various tectonic settings (compressional, extensional, and strike-slip/oblique-slip) (Chen et al. 2003; Cyr et al. 2010; El Hamdouni et al. 2008; Krystopowicz et al. 2020; Rimando and Schoenbohm 2020; van der Wal et al. 2020; Yildirim 2014). To investigate the relative tectonic activity and relative uplift rates of the OBG, four geomorphic indices were used and integrated with the analysis of a swath profile and local relief map. The geomorphic indices that were collected include valley floor width-to-valley height ratio (V_f), basin elongation ratio (R_e), basin hypsometric integral (HI), and normalized channel steepness index (k_{sn}). Schematic diagrams of the drainage basins and the different measurement procedures are compiled in Fig. 4.

Fig. 2. Seismicity in the Ottawa-Bonnechere Graben. (a) Earthquake epicentral plot from the eastern Canada earthquake bulletin from 1930–2022 with earthquake magnitude from 3 to 6 (red dots = M5–6, orange dots = M4–4.9, and green dots = M3–3.9) (<https://earthquakescanada.nrcan.gc.ca/index-en.php>) plotted on a 30 m ASTER global digital elevation model (<https://doi.org/10.5067/ASTER/ASTGTM.003>). Black lines are fault lines from Lamontagne et al. (2020). (b) Earthquake focal mechanisms plotted with red and white beachball and labelled with year and magnitude. Focal mechanism solutions are from Bent et al. (2002, 2003, 2015); Du et al. (2003); Ma et al. (2008).



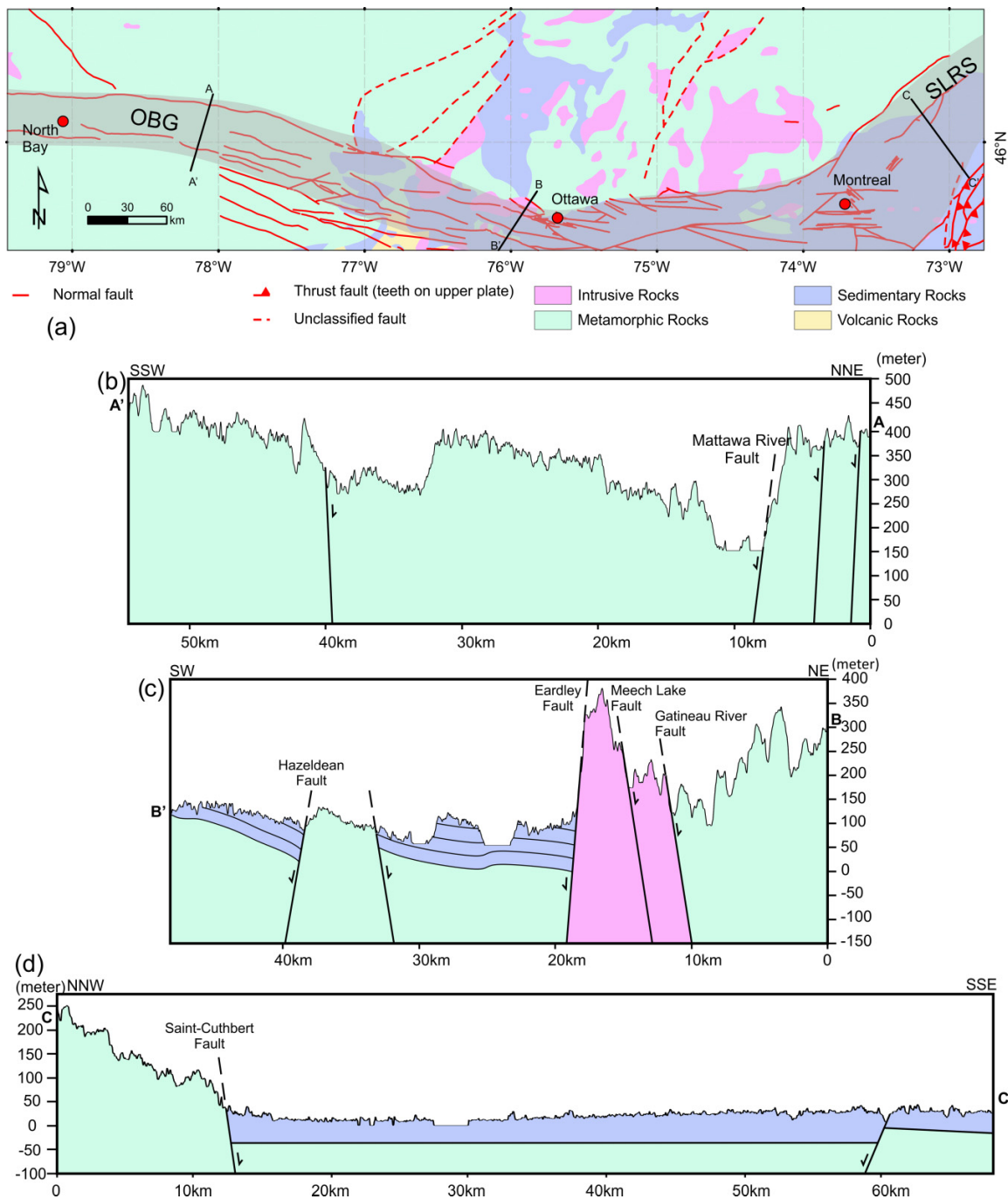
We performed a morphotectonic analysis of drainage basins along ~629 km of the OBG to obtain quantitative information regarding the spatial distribution of relative tectonic uplift rates in the region. The OBG is characterized by a low relief landscape with elevation that is generally <500 m, with the most significant morphological feature being the Gatineau hills escarpment (Fig. 1). This bedrock escarpment extends from North Bay to Joliette (Fig. 1), trends northwest-southeast, and lies parallel to the main Ottawa River. Morphometric indices were measured in the northern segment of the OBG because it has a clearly defined bedrock escarpment. However, measuring geomorphic indices in the OBG is challenging because the area has a low relief due to glacial peneplanation (Dyke et al. 2002) and because the drainage system on the hanging-wall is an alluvium river rather than a bedrock river, making geomorphic indices measurement unreliable. Another factor to consider while determining the appropriate location to measure geomorphic indices on and to properly explain the uplift rates is determining the hanging-wall under the current fault kinematics. In our case, while the current landform resembles rift morphology, which is made up of a series of normal faults, the bedrock escarpments are thought to be the footwall blocks of reverse faults that occupy the northern portion of the OBG. Because of this, the

relative uplift rates may not be directly related to the activity of the bedrock scarp-forming OBG structures.

Swath profiles were used to corroborate the characterization of relative uplift rates from tectonic geomorphology indices analysis, as in previous studies (Telbisz et al. 2013; Yıldırım 2014; Wang et al. 2019). A 20-km-wide topographic swath profile of the east-west-trending OBG bedrock escarpment was created (Fig. 5). Swath topographic profiles extracted across the OBG bedrock escarpment illustrate the elevation distribution along its length. Along-strike swath elevation profiles have been demonstrated to be useful in estimating cumulative fault throw and lateral differential uplift rate (Telbisz et al. 2013; Yıldırım 2014). In this study, two geomorphic indices (H_i and R_e), which reflect drainage basins morphological properties, and two indices (V_f and k_{sn}) which reflect stream channel geometrical properties, were analysed (Fig. 4). Tectonic activity then classified by cross-correlating the four geomorphic indices.

The drainage basins in proximity to the northern arm of the OBG area were divided into six sections, referred to here as sections 1–6. The region was divided into sections based on the existence of fault-related topographic troughs in the swath profiles, and changes in fault strike coinciding with changes in escarpment orientation (Fig. 5). The division of the

Fig. 3. (a) Generalized geological map of Ottawa-Bonnechere Graben (OBG) modified from Geological Map of Canada Map D1860A (1996) (<http://geoscience.nrcan.gc.ca/>) and overlaid by faults from Lamontagne et al. (2020) and geologic cross sections of (b) the western section A'-A, (c) middle section B'-B, and (d) eastern section of OBG C'-C.

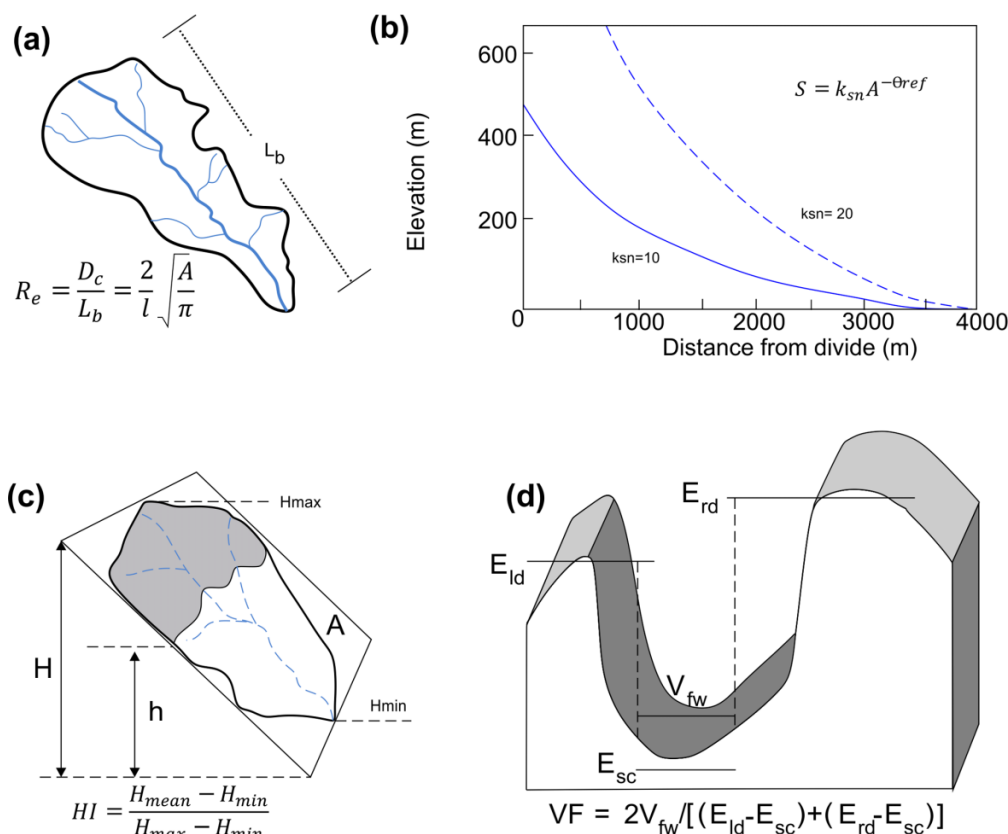


sections was also correlated to the faults and lineaments compilation of the OBG from Lamontagne et al. (2020) such that section 1 corresponds to the Mattawa River Fault, section 2 to the Coulange Fault, section 3 to the Eardley Fault, section 4 to the Gatineau Fault, section 5 to the Lachute and New Glasgow Faults, and section 6 to the Sainte-Julienne and Saint-Maurice Faults. Sections 5 and 6 consisted of two faults, respectively, but those faults showed no topographic expression and had the same orientation in these sections. The section division

along fault segments was also aimed to identify the role of pre-existing faults to possibly exhibit relatively high tectonic activity and record spatial variation in high uplift rates.

We used the Jet Propulsion Laboratory National Aeronautics and Space Administration's open-access Advanced Spaceborne Thermal Emission and Reflection Radiometer (ASTER) Global Digital Elevation Model Version 3 (GDEM V3). ASTER GDEM V3 has a spatial resolution of 30 m and can be downloaded from <https://asterweb.jpl.nasa.gov/gdem.asp>

Fig. 4. Diagrams of various geomorphic indices including the formulas that were used to calculate the uplift rate modified after Bull and McFadden, (1977); Cheng et al. (2018); Rimando and Schoenbohm (2020). (a) Basin elongation ratio (R_e). (b) Channel steepness index (k_{sn}). (c) Hypsometric integral (HI) that shows the normalized elevation. (d) Valley floor width-to-height ratio (V_f).



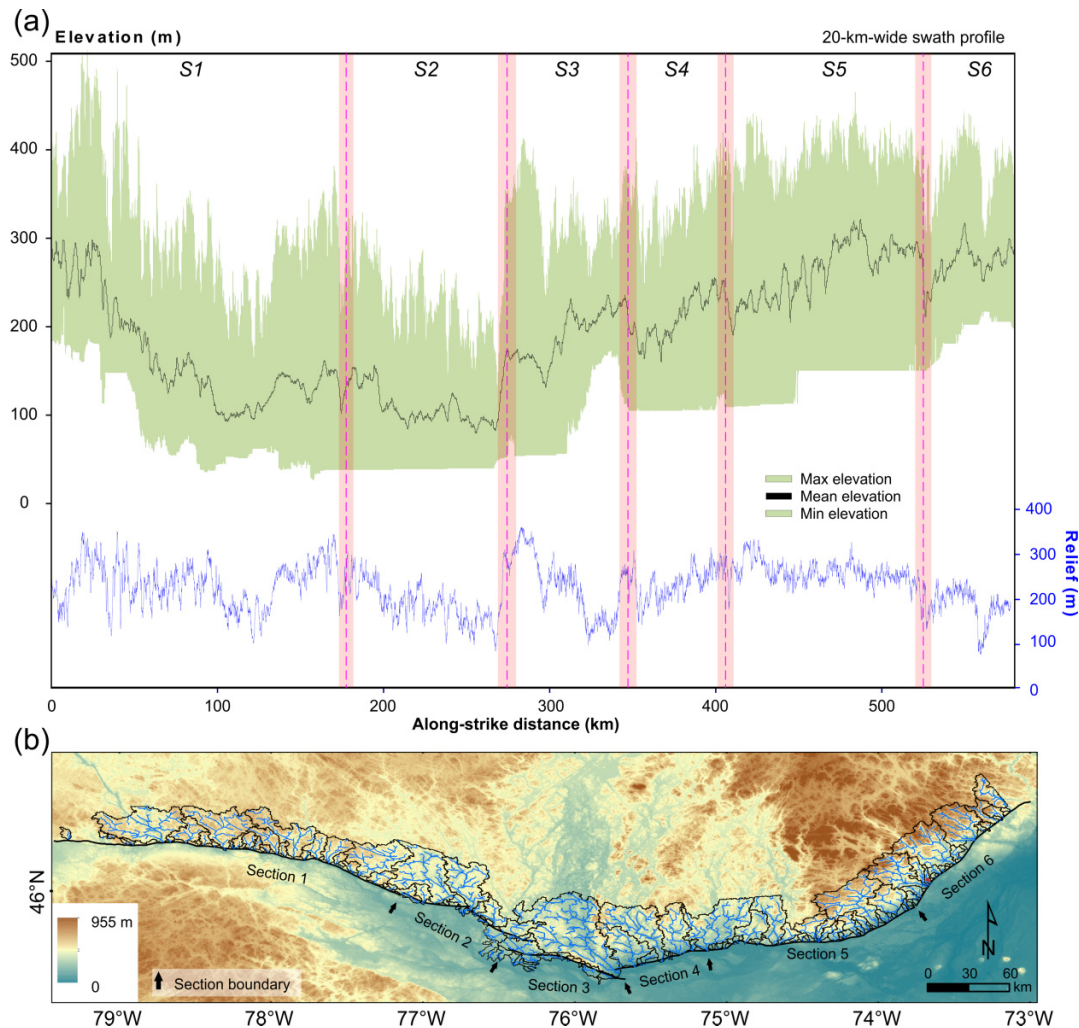
(NASA/METI/AIST/Japan Space Systems and U.S./Japan ASTER Science Team, 2019). It served as the primary data to map and characterize drainage basins, which is then used in this study as a proxy to understand the long-term deformation history of the OBG. A total of 131 drainage basins that cover the northern arm segment of the OBG were analysed (Fig. 5, Table S1 in Supplementary Material). However, because the bedrock escarpment only occurs prominently along the northern side of the OBG, morphotectonic analysis could only be performed in this location (Fig. 1). The graben is a relict of the previous rifting that is overlaid by Palaeozoic sedimentary rocks (Sanford 1993; Oruche et al. 2018) which are more prone to erosion, and which lacks a substantial bedrock escarpment in the southern section (Figs. 3 and 5). Previous research has demonstrated that a single geomorphic index is insufficient to reliably infer relative uplift rates in a vast region, such as the one studied here, because uplift rates can be affected by variety of conditions, including lithological variation, which affects erosional resistance (Clayton and Shamoon 1998; Bucci and Schoenbohm 2022; Selby 1980; Telbisz et al. 2013).

Lithological variation plays an important role in determining the spatial distribution of rock erosional resistance, which is a critical aspect in measuring geomorphic indices (Kühni and Pfiffner 2001). In this study, rock erodibility was

not measured directly in the field. Rather, the findings of previous studies that used lithology to infer rock erodibility were incorporated (Kühni and Pfiffner 2001; Korup 2008; Jansen et al. 2010; Wolpert and Forte 2021). A regional geological map (Wheeler et al. 1996) (Fig. 3) was used to infer the rock erosional resistance level using the rock erodibility ranking from previous studies (Selby 1980; Clayton and Shamoon 1998). In this study area, crystalline metamorphic and igneous rocks were characterized as strong, while the sedimentary rocks were characterized as moderately weak and more susceptible to erosion and weathering.

We used Google maps satellite images (2019–2020) (<https://earth.google.com/web/>) and an integration of hillshade and colour-coded classified slope maps generated from the ASTER GDEM. Previous studies show that ASTER GDEM has been effectively used in morphotectonic analysis to assess relative tectonic activity in various geological settings due to its extensive global coverage and its sufficient vertical and horizontal accuracy for the purpose of morphotectonic studies (Radaideh et al. 2016; Xue et al. 2018; Rimando and Schoenbohm 2020; Krystopowicz et al. 2020). The DEM was also used to quantify local relief and was used to measure the normalized channel steepness index. Following the methods outlined in Marliyani et al. (2016), a 2.5 km radius sampling window was used to calculate local relief, which is a reason-

Fig. 5. (a) Swath profiles along west–east Ottawa-Bonnechere Graben along major fault features in black lines from Lamontagne et al. (2020) plotted on a 30 m ASTER global digital elevation model (<https://doi.org/10.5067/ASTER/ASTGTM.003>). (b) Drainage basins with black polygons and blue lines as rivers distributed along fault lines in the northern arm of the OBG (represented by black lines). Black arrows indicated the drainage section divide and fault borders. Drainage basins numbering can be seen on Fig. S1 in Supplementary Material.



able size given that rock type variation was not significant in the area where the geomorphic indices were measured (Fig. 3). In areas with complex lithological variation, decreasing the sampling radius could be used to minimize the effect of lithological controls on landform modification, as local relief is a scale-dependent measurement (DiBiase et al. 2010; Marliyani et al. 2016). The resampled elevation of local relief was used to identify morphological elements (Marliyani et al. 2016). The geological map of the OBG modified from Wheeler et al. (1996) was also integrated into the database to provide the distribution of rock units and structural information for tectonic geomorphology interpretation (Fig. 3).

The DEM was analysed using the Spatial Analyst Tool in the ArcMap-ArcGIS 10.8 software package to provide watershed properties such as flow direction, flow accumulation, stream network, and drainage basin geometry (Rimando and Schoenbohm 2020; Krystopowicz et al. 2020). To define and extract drainage basin (watershed) and stream network data,

first, sinks, or holes in the DEM were filled as these represent potential sources of error (Gailleton et al. 2021). The flow direction was determined by comparing each cell to its steepest downslope neighbour. The next step was to generate a flow accumulation map (i.e., generating a river pattern from DEM) by computing the weight of all cells that accumulated into each nearby downslope cell (~30 m ASTER GDEM cell size) (Rimando and Schoenbohm 2020). The geometry of the drainage basins was extracted by locating pour points at the intersection between the trace of the bedrock fault escarpments and the river channels that drained from upslope as in Rimando and Schoenbohm (2020). The extraction of this data was achieved by computing all the upslope cells that drain into high accumulation cells. This generated watersheds rasters, which were then transformed to shapefiles and clipped to each watershed (Fig. 5). Each of the clipped watersheds has information on the basin's length, width, area, maximum and minimum elevation. The drainage basins were

filtered to only include those with areas greater than 2.5 km² to avoid analysis of nonfluvial process and DEM artifacts or other errors. The reason for this is that measuring smaller area basins could lead to unreliable results as the basins were too young to record the tectonic processes of interest (Bull and McFadden 1977).

3.1. Valley floor width-to-valley height ratio

V_f is the comparison between valley floor width and the mean of valley floor height given by the following equation (Bull 2008):

$$(1) \quad V_f = \frac{2V_{fw}}{(E_{ld} - E_{sc}) + (E_{rd} - E_{sc})}$$

where V_{fw} is the width of the valley floor; E_{ld} and E_{rd} are the elevations of the left and right sides of the valley, respectively; and E_{sc} is the mean elevation of the valley floor. V_f values <0.5 imply a narrow, dominant vertical erosion, manifesting as a deeply incised and V-shaped valley geometry which could be a signal of very high uplift rates. On the other hand, values >0.5 or closer to or greater than 1 indicate a U-shaped valley that is associated mainly with lateral erosion, which is indicative of low uplift rates (Bull 2008).

V_f was measured in ArcGIS using the “interpolate line” and “profile graph” functions to create elevation cross-sections of the selected drainage basins. On average, the valley floors are narrow (Bull and McFadden 1977; Baharvand et al. 2020) upstream and wider downstream; standard distance of around 0.5–1 km upslope was therefore applied to measure V_f from bedrock escarpment-related drainage basins (Fig. 4) (Bull and McFadden 1977).

3.2. Basin elongation ratio

Basin elongation ratio is the ratio between a basin longest axis and a basin’s width or the diameter of a circle with the same area as the basin (Schumm 1956). Tectonically active drainage basins typically manifest as actively rising topography which is highlighted by elongate geometry, and inactive basins tend to be more oval-circular as lateral migration and stream dispersion take place (Cannon 1976; Ramírez-Herrera 1998; Bull 2008).

Basin elongation (R_e) is defined by the equation (Schumm 1956):

$$(2) \quad R_e = \frac{D_c}{L_b} = \frac{2}{l} \sqrt{\frac{A}{\pi}}$$

where L_b is the drainage basin’s maximum length, the diameter of a circle with the same area as the basin is D_c , and A is the drainage basin coverage area. The shape geometry is classified as follows: circular (0.9–1.0), oval (0.8–0.9), slightly elongated (0.7–0.8), elongated (0.5–0.7), and very elongated (<0.5) (Strahler 1952; Rimando and Schoenbohm 2020). While basin elongation values (0.6–1.0) have a variety of climatic and lithological control, elongated basins ($R_e = 0.6–0.8$) are usually characterized by areas of moderate to high relief and steep slopes and are associated with a high relative uplift rate, and circular basins with R_e values close to 1 (Strahler 1952)

are characterized by flat relief and gentle slopes, and are likely associated with low uplift rate (Fig. 4) (Strahler 1952).

To measure the length of each drainage basin, a minimum bounding geometry (MBG) function was obtained using ArcGIS. The MBG function creates polygons that enclose watersheds and provides the length, width, and area for these. The areas of drainage basins were extracted from the attribute table of each drainage basin polygon.

3.3. Hypsometric integral

Hypsometric integral (HI) is the subarea below the hypsometric curve, which can be used to infer the basin maturity and the amount of bedrock material that has not been eroded (Strahler 1952). The hypsometric curve is a plot between normalized cumulative area and normalized relief, plotted on the x and y axes, respectively. The curve explains the elevation distribution of landscapes of various sizes, including watersheds or drainage basins. HI is calculated using the following equation (Strahler 1952):

$$(3) \quad HI = \frac{H_{mean} - H_{min}}{H_{max} - H_{min}}$$

where H_{mean} , H_{max} , and H_{min} are the mean, maximum, and minimum elevation, respectively. HI values can be used to characterize maturity and erosional stage of the drainage basins (Strahler 1952; El Hamdouni et al. 2008). HI values usually range from 0 to 1, with late-stage or mature basins associated with a value of 0.5 (Carson and Kirkby 1972) or 0.6 (Chorley 1971). Other studies characterized drainage basins with HI values of <0.30 as belonging to a mature stage, with erosion dominating in higher elevation, and likely exhibiting relatively low or stable uplift rates (Strahler 1952; Keller and Pinter 1987). On the other hand, HI values >0.60 indicate less erosion at high elevations, and are associated of a young landscape, typically because relative high uplift rates cause rejuvenation (Fig. 4) (Strahler 1952; Keller and Pinter 1987; Chen et al. 2003). A high HI value indicates a broad-elevated surface with minimal erosion and therefore implies an immature landscape produced by high relative uplift rates, while lower HI suggests isolated elevated surface produced by low uplift rates (Lifton and Chase 1992; Chen et al. 2003). For this study, statistical derivation of the HI was computed using the open source CalHypso add-in toolbox for ArcGIS (ESRI) developed by Pérez-Peña et al. (2009) from the DEM of each drainage basin.

3.4. Normalized channel steepness index

k_{sn} (normalized channel steepness index) is a DEM-derived longitudinal profile of bedrock channel slope that has been normalized to drainage basin area (Kirby et al. 2003; Wobus et al. 2006; Cyr et al. 2010). k_{sn} is a well-established method and has been widely used to map spatial distribution and/or variation of relative uplift rates in various landscape settings (Snyder et al. 2000; Kirby et al. 2003; Wobus et al. 2006; Cyr et al. 2010; Mathew et al. 2016a). k_{sn} has been widely applied in various tectonic settings (e.g., inversion, collision, subduction) to infer the pattern of relative uplift rates along fault

systems (e.g., Kirby et al. 2003; Cyr et al. 2010; Wang et al. 2019; Rimando and Schoenbohm 2020).

k_{sn} is based on the stream power incision model that is expressed by the following equation (Snyder et al. 2000):

$$(4) \quad S = k_{sn} A^{-\Theta_{ref}}$$

where S denotes the steepness of channel in slope value, A is the upslope catchment area, and Θ_{ref} is the drainage basin's concavity. The range of river concavity in nature is from 0.4 to 0.6, with 0.45 used as the standard reference concavity value (Fig. 4) (Snyder et al. 2000; Kirby et al. 2003; Wobus et al. 2006; Marliyani et al. 2016). The reference concavity ($\Theta_{ref} = 0.45$) is assumed as a good approximation of natural river concavity (Snyder et al. 2000; Kirby et al. 2003; Kirby and Whipple 2012). According to Mudd et al. (2018), if a higher Θ_{ref} is chosen, the entire channel network can have similar channel steepness, or if a lower Θ_{ref} is chosen, the lower drainage portion can have high channel steepness. In various tectonic and geologic settings with variable climatic regimes and rock types, a linear relationship between k_{sn} and uplift rate has been demonstrated (Snyder et al. 2000; Wobus et al. 2006; Cyr et al. 2010; DiBiase et al. 2010; Kirby and Whipple 2012). However, the channel steepness index can also be affected by local erosion and discharge (Tucker 2004). Therefore, k_{sn} can be utilized to map spatial and/or temporal patterns or variation in uplift in areas with generally consistent rock erosional resistance and climate (Wobus et al. 2006; Kirby and Whipple 2012; Whipple et al. 2013). Therefore, to better characterize spatial distribution of relative uplift rate using k_{sn} values, several parameters should be considered that may contribute to uplift rate variation such as lithologic contrast (Cyr et al. 2010; Duvall 2004; Hack 1973), precipitation rate (e.g., Bookhagen and Strecker 2012), and stream capture (Robl et al. 2017).

The k_{sn} calculation was undertaken in MATLAB using the TopoToolBox program (Schwanghart and Scherler 2014) with ASTER GDEM V3 as input. The flow direction and flow accumulation were calculated using a threshold upstream area of 5 km² and smoothing factor of 100. The results were then imported to ArcGIS as a shapefile and converted to raster and the swath profile with a radius distance of 5 km was performed to capture k_{sn} values along fault lines.

3.5. Relative tectonic activity analysis

Relative levels of tectonic activity can be inferred by using an integration of analyses of the landscape, including drainage basins (Bull and McFadden 1977; El Hamdouni et al. 2008; Yıldırım 2014). To describe the level of Quaternary relative tectonic activity (high, moderate, low), previous researchers have tried to integrate various geomorphic indices (El Hamdouni et al. 2008; Saber et al. 2020). Cross-correlation between multiple geomorphic indices and topographic parameters, were performed to translate each index into a tectonic activity class. Cut-off values were assigned to each individual geomorphic index to classify the corresponding relative uplift rates. However, the boundary values between different classes of each index vary according to the lithological variation and structural setting as in previous work (Rockwell and Keller 1985; Bull 2008). The geomorphic in-

dices were measured on bedrock escarpments with relatively uniform rock erosional resistance (mostly gneiss) (Fig. 1) and climatic conditions. As such, we applied the relative tectonic classification and boundary values from El Hamdouni et al. (2008) and Cheng et al. (2018). Three relative tectonic activity classes were defined: (1) high uplift rates, (2) moderate uplift rates, and (3) relatively low uplift rates. Class 1 has HI > 0.5, V_f < 0.5, R_e < 0.6, and k_{sn} > 150; class 2 has HI 0.4–0.5, V_f 0.5–1, R_e 0.6–0.8, and k_{sn} 50–150; and class 3 has HI < 0.4, V_f > 1, R_e > 0.8, and k_{sn} < 50. Along-strike plotting of these indices was done by combining HI, V_f , R_e , and k_{sn} values of each drainage basin.

4. Results

The results of our measurement of four geomorphic indices in the OBG are described in this section (Figs. 6, 7, and S2 and Table S1 in Supplementary Material). The geomorphic index results are plotted against the distance along the escarpment. The standard deviation lines (maximum and minimum) are plotted to help with depicting spatial variation of indices and identifying the high and low sections/drainage basins.

4.1. Valley width-to-height ratios

The mean V_f values obtained range from 0.2 to 2.3 along the six drainage sections of the OBG's bedrock escarpment (Figs. 6 and 7). These values indicate that most of the valleys are "V" shaped with dominant vertical incision. V_f values suggesting "U"-shaped valleys were observed three times, in sections 2–4 (Figs. 5 and 6). In the eastern (1 and 2) and western sections (3, 4 and 5), low V_f values were observed with a range around 0.5. Furthermore, moderate V_f values (0.5–1.0) are observed in some parts of sections 3 and 4 (Fig. 6). Most of the V_f values are between the standard deviation lines. There are a total of five values that are depart from the average, two of which are in section 1 and one each in sections 3–5.

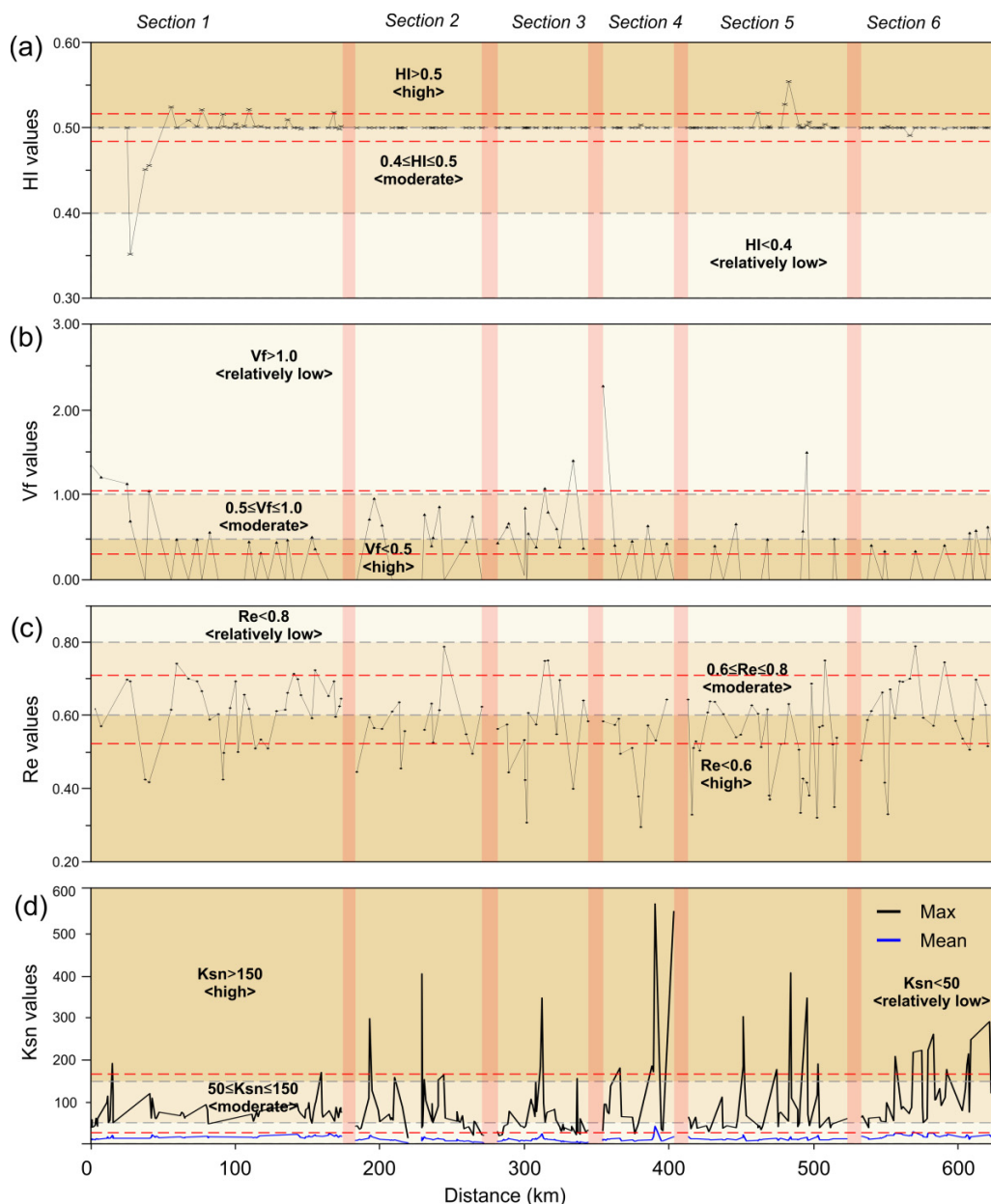
4.2. Basin elongation ratio

The basin elongation ratio (R_e) values obtained range from 0.38 to 0.81 along the OBG (Figs. 1, 6, and 7). R_e values were found to be mostly less than 0.6 along the east–west transect of the OBG. A low number of watersheds with R_e values ranging from 0.7 to 0.8 occur locally along west–east transects of the OBG (Fig. 6). Sections 2–5 of the OBG, are dominated by very elongated (0.5–0.7), while sections 1 and 6 display mostly elongated (0.5) basins. Most of the drainage basins in sections 1, 2, and 4 have elongation ratio values between the standard deviation lines. However, in sections 3, 5, and 6, a total of 24 drainage basins have basin elongation ratio values lower than the lower boundary of standard deviation lines.

4.3. Hypsometric integral

Hypsometric integral (HI) values obtained range from 0.35 to 0.55 with a mean HI of 0.50 for the six sections in the OBG (Figs. 1, 6, and 7). The lowest HI value (0.35) obtained is in section 1 where two large rivers merge: the northwest–southeast-trending Ottawa River and east–west Mattawa River (Figs. 2, 6, and 7). The highest HI, with a value of 0.55 in section 5, spatially coincides with the northwest–

Fig. 6. Geomorphic indices profiles of a west–east section in bedrock fault escarpments. The bedrock escarpments are divided into six sections (Fig. 5): S1, section 1; S2, section 2; S3, section 3; S4, section 4; S5, section 5; and S6, section 6. Values from the six sections are separated by red-shaded regions. (a) Hypsometric HI, (b) valley-floor-width-to-height (V_f) ratio, (c) basin elongation ratio (R_e), and (d) channel steepness index (k_{sn}). The dashed grey lines reflect the cut-off value for high or low uplift rate. The colours of medium to light brown reflect high, moderate, and low uplift rate values. Dashed red lines are the standard deviation of each index.



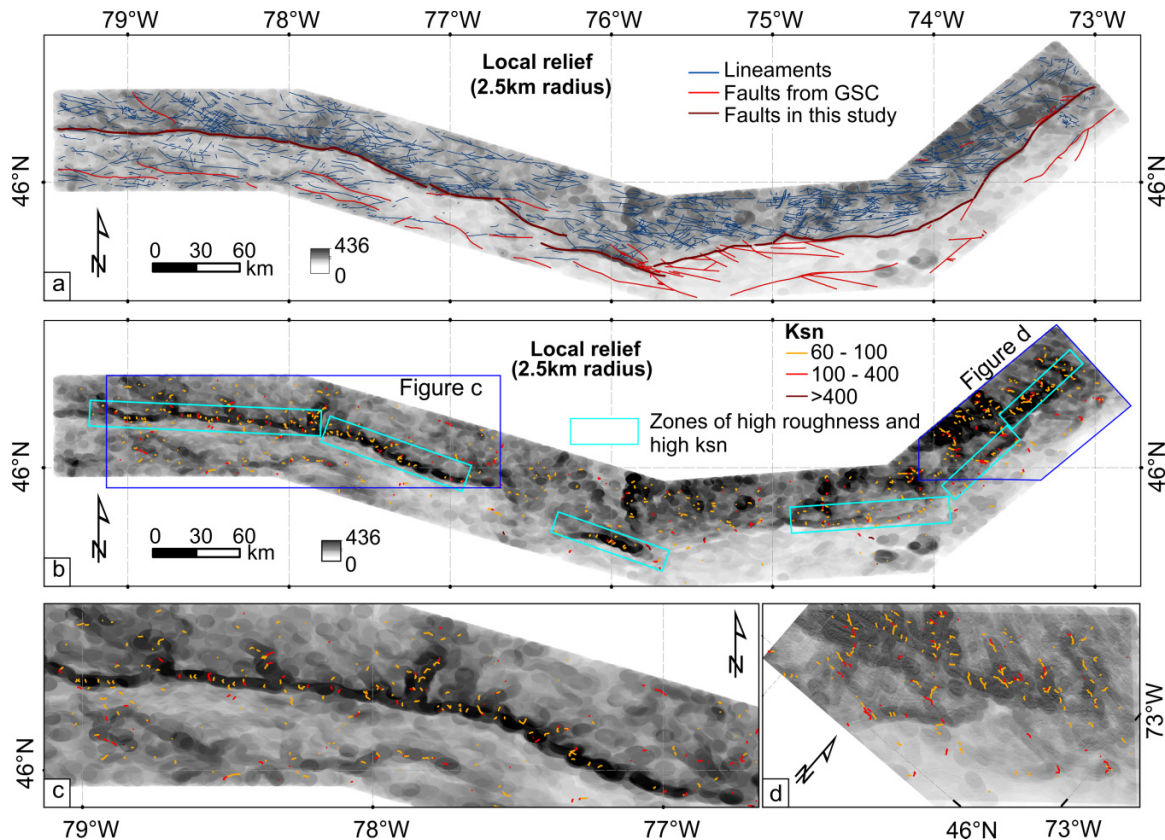
southeast band of seismicity. The majority of the drainage basins in the OBG have HI values of 0.5 (Fig. 6). Only five of the drainage basins, three in section 1 and two in section 5, have HI values outside the standard deviation range. In section 1, those three drainage basins have relatively lower values while in section 5 the values are higher than the mean.

4.4. Normalized channel steepness index

The k_{sn} values obtained from the river profiles in the study area range from <50 to >400. The high k_{sn} values are mostly

found in tributary rivers that flow into the main Ottawa River, which runs along or parallel to the Palaeozoic faults (Figs. 6 and 7). While the lowest k_{sn} values are located mostly in section 1 and the western part of section 3. The low values are in the hanging wall block that forms the Ottawa River valley, and the upslope area along the northern side of the river. Generally, between these two low k_{sn} values (<60), the k_{sn} values increase significantly toward the OBG's bedrock escarpments in other sections, which corresponds with the zone of high local relief. Spatial distribution of the high k_{sn} values (>60) shows no along-strike variation (Figs. 6 and 7). Five out of the

Fig. 7. Compiled channel steepness analysis (k_{sn}) in Ottawa-Bonnechere Graben (refer to Fig. 1 for location). Full result of k_{sn} is available in Fig. S2. (a) The structural distribution map shows faults in this study, interpreted lineaments, and other faults (Lamontagne et al. 2020) overlaid on local relief displayed using a 2.5 km sampling radius. (b) Map of the spatial distribution of k_{sn} with the red-coloured channel lines with indicated high k_{sn} value; high local relief is represented with black; note the overriding high k_{sn} and high local relief highlighted in the light blue box while dark blue box indicated the zoom-in of Figs. 6c and 6d. (c) The western segment of OBG included the Mattawa River Fault and Coulonge Fault. (d) The eastern segment of OBG covered Saint-Maurice Fault.



six sections have k_{sn} values higher than the standard deviation range derived from maximum k_{sn} values, with section 1 being the exception. Sections 2–6 have k_{sn} values ranging from more than 200 to ~600 that are categorized as high. Most of drainage basins in section 1 have k_{sn} values that fall within the standard deviation range (Fig. 6d).

4.5. Relative tectonic activity

HI values are typically around 0.5, which represents the threshold between moderate and strong uplift rates. In numerous locations, HI was >0.5 , meaning these areas are undergoing relatively high uplift. The majority of the V_f values are <0.5 , indicating a relatively high uplift rate, while the remaining V_f values calculated have moderate uplift rates ranging from 0.5 to 1. The R_e value varies from 0.3 to 0.78, indicating a moderate to relatively high uplift rate. Most of these values are below 0.6 and are therefore classified as having a relatively high uplift rate. k_{sn} values range from 0 to >500 , with most displaying a moderate uplift rate ranging from 50 to 150. High k_{sn} values of more than 150–500 were recorded in several rivers and are categorized as regions with a relatively high uplift rate. Most of the drainage basins in sections 2–6

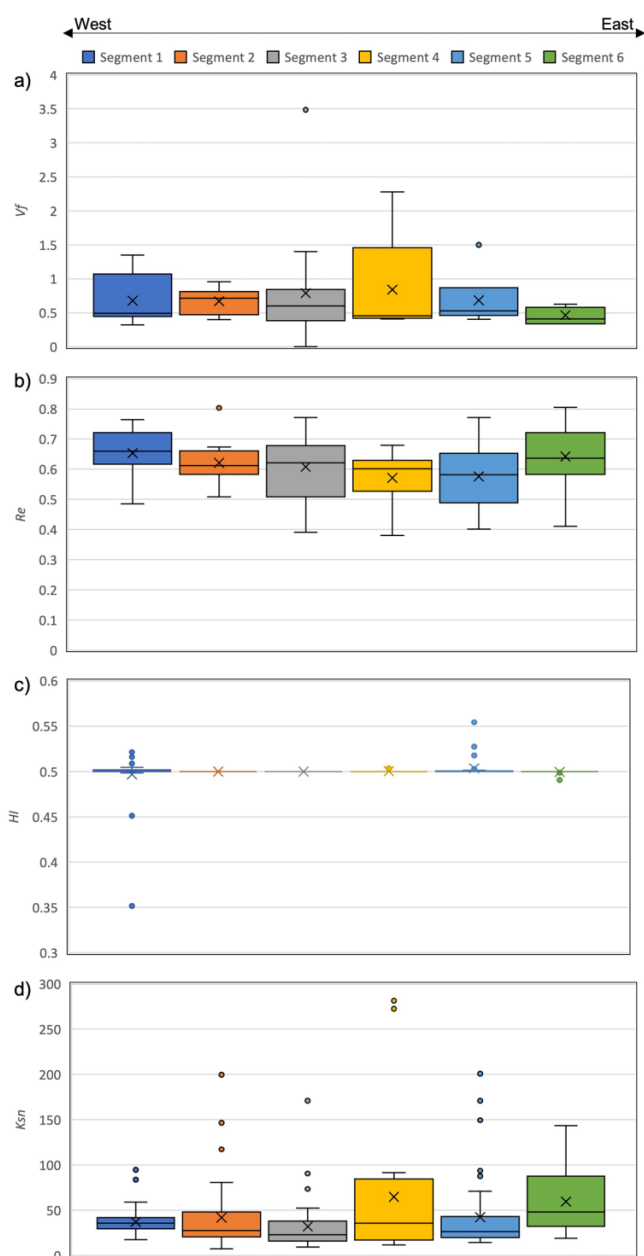
show signals of high relative tectonic activity while drainage basins in section 1 showed moderate relative tectonic activity.

5. Discussion

5.1. Geomorphic proxies and relative tectonic uplift rates along the Ottawa-Bonnechere Graben

The impact of tectonic activity in the OBG upon the geomorphology has been observed and quantified through the calculation of multiple geomorphic indices (Figs. 6–8). This is particularly valuable in OBG where this assessment of neotectonic activity using a morphotectonic approach is the first of its kind. Analysis of multiple geomorphic indices including V_f , R_e , HI, and k_{sn} has provided indications of high relative uplift rates and ongoing long-term regional deformation (Figs. 6 and 7). The high k_{sn} values indicate a relatively high rates of vertical incision. For example, compared to sections 1 and 2, sections 3–6 have higher steepness index indicating disequilibrium which is likely associated with ongoing relative

Fig. 8. Box-whisker plots of morphometric indices analysis summary (from top to bottom: (a) valley floor-to-width ratio (V_f), (b) basin elongation ratio (R_e), (c) hypsometric integral (HI), and (d) normalized channel steepness index (k_{sn})) along the strike of the Ottawa-Bonnechere Graben. Box-whisker plot represents the lower (25th percentile) and upper (75th percentile) cut-off values. The median values are represented by black lines and the mean values are represented by X shapes. The k_{sn} data in these boxplots were collected from the median value of k_{sn} of each catchment from swath profile.



uplift processes (Figs. 6 and 7). Most of the geomorphic proxies show high values which reflect high relative uplift rates within the OBG (Figs. 6 and 7a–7c).

Applying several previously defined geomorphic indices boundary values to define uplift rates (low, medium, and

high) (Bull and McFadden 1977; El Hamdouni et al. 2008; Cheng et al. 2018; Rimando and Schoenbohm 2020; Saber et al. 2020) reveal that each section of the OBG drainage basins correspond to inferred high relative uplift rates. Morphometric analysis can be used to correlate river responses to uplift rates and fault slip rates. For example, in the Himalayan fold and thrust belt the shortening rate due to convergence has been shown in river responses (Wahyudi et al. 2021). Although, in the OBG, the relative uplift rates does not correspond directly with fault slip rate, they can provide insight into the spatial distribution and variation of relative uplift rates (Chen et al. 2003; Bull 2008; Boulton 2020). This is best characterized by sections 1 and 2 in the western sections and sections 5 and 6 in the eastern sections. In this context, sections 3 and 4, which are characterized by relatively high local relief, high channel steepness, and convex basin geometry, likely indicate a dominantly vertical channel steepening process that is likely associated with high relative uplift rates. Cycles of glacial retreat and advance during the Pleistocene could also have potentially influenced the k_{sn} in the OBG (Dyke et al. 2002). For example, ice melt during glacial retreat may have increased water volume, resulting in more energetic rivers and glaciers which were more erosive, resulting in increased erosion rates and creating higher channel steepness (Brocklehurst and Whipple 2007; Sternai et al. 2011).

The HI profiles generated along the OBG present relatively constant values of around 0.5 which indicates denuded topography (Figs. 6 and 7) (Strahler 1952; Kirby et al. 2003; Chen et al. 2003), or potentially broad-scale erosion by deglaciation (Dyke et al. 2002). We interpret this result to be a product of peneplanation during glaciation that eroded and flattened the morphology in the study area (Dyke et al. 2002). The lowest HI values are located at the intersection between the Ottawa River and Timiskaming River, which has a wider elevated valley floor surface compared to other drainage basins and is dominated by denudational processes. We observed that along with the mid to eastern section (sections 4–6) (Fig. 6) of the OBG, most of the high k_{sn} values correspond to lithological variation separated by faults. While many of the k_{sn} values in the west section (sections 1 and 2) (Fig. 6) to sections 3 and 4 are located along previously mapped and interpreted faults (Lamontagne et al. 2020) without lithological variation, some k_{sn} neither have any apparent lithological contrast or fault control (Figs. 6 and 7). Aside from lithological variation, variation of rock strength might also influence the k_{sn} and V_f results, as Selby (1980) notes that the rock mass strength can affect the state of rock weathering, and the intensity and orientation of joints and fractures.

5.2. Spatial distribution of regional relative uplift rates revealed in the Ottawa-Bonnechere Graben

Our k_{sn} and V_f results show that the northern arm of the OBG bedrock escarpment has a high relative uplift rate. The morphometric data exhibit high-values from, west to east with no significant spatial variation (Figs. 6–8). The R_e values obtained indicate that the elongate drainage basin shape is a

result of low lateral erosion likely due to active uplift. Our results extend the temporal range of uplift rate observations as the morphometric data obtained represent long-term deformation. By contrast, GPS data allows short-term and ongoing deformation to be quantified. The short-term deformation can be seen on the seismicity distribution and vertical uplift from GPS.

Our morphotectonic activity analysis reveals relatively high uplift rates throughout the OBG. The local relief maps show high relief values that correspond to high k_{sn} values located at previously mapped fault traces from sections 1 to 6 (Fig. 7). The OBG fault zone is an aulacogen dominated by vertical slip and a poorly constrained lateral component (Wallach et al. 1995; Tremblay et al. 2003; Rimando and Benn 2005; Rimando and Peace 2021). According to seismology and Quaternary sedimentology studies, faults in the OBG are undergoing reactivation under the present-day stress regime (Bent 1996a; Brooks 2020; Doughty et al. 2010a, b; Ma et al. 2008). The Canadian Base Network GPS shows approximately 1–2 mm year⁻¹ broad regional uplift in the OBG that exhibits a spatial uplift pattern indicating glacial unloading (Henton et al. 2006). Our results depict a consistent and symmetrical relatively high uplift signal along the OBG (Figs. 6 and 8) that we interpret as a broad wavelength regional uplift. The broad wavelength regional uplift involves an area on the order of hundreds of kilometres. GIA has been proposed to play an important role in creating an uplift signal and that supposedly trigger the reactivation of pre-existing structures (Wu and Hasegawa 1996), while tectonic stress has also been considered as another causal mechanism (Wu and Hasegawa 1996; Rimando and Peace 2021). While glacial unloading could be a plausible cause of recent seismicity in the OBG, an alternative theory postulates that the Mesozoic Great Meteor Hotspot (GMH) might be the cause of the present-day seismicity. This theory proposes that the GMH traversed the region along an approximately northwest–southeast-trending track weakening the inherited rift structures, and thus contributing to present-day linear seismicity in the OBG (Adams and Basham 1989; Dineva et al. 2007; Ma and Eaton 2007). However, Rimando and Peace (2021) claim that shallow seismicity (<8 km), appears to be more randomly distributed throughout the region and highlight that it is not clear why seismicity would be sustained to the present-day through this thermal weakening mechanism. Overall, comparison of our result to the GPS uplift rate confirms our interpretation that the area is subject to both long- and short-term broad wavelength regional uplift.

5.3. Implications on regional uplift and intraplate seismicity

The level of seismic hazards and risks in intraplate regions are low compared to high-strain regions characterized by more frequent and higher magnitude earthquakes (Yu et al. 2016; Ojo et al. 2021). Nonetheless, recent and historical destructive earthquakes in other cratonic regions, e.g., Australia (Gold et al. 2019; King et al. 2021), China (Kirby et al. 2008; Fielding et al. 2013b), and Turkey (Elliott et al. 2013; Fielding et al. 2013a) demonstrate the necessity of seismic

hazard and risk assessment studies in regions such as eastern Canada.

Comparing our results with previous GPS studies provides further insight into the regional uplift and intraplate seismicity. While GPS time-series measurements indicate that the contemporary strain rate in the OBG is relatively low (Sella et al. 2007; Alinia et al. 2017), the GPS time series reveal that vertical velocities vary spatially, with uplift predominantly occurring in the Hudson Bay region to the north, and mostly subsidence occurring in the Great Lakes region to the south (Mazzotti et al. 2005; Alinia et al. 2017; Sella et al. 2007; Tarayoun et al. 2018). Therefore, if pre-existing faults in the northern arm of OBG are reactivated through broad regional uplift, resultant seismicity could affect areas which includes cities such as Ottawa, Gatineau, and Montreal (Figs. 2 and 3). For instance, under the northwest–southeast-trending maximum horizontal current stress regime (Mazzotti and Townend 2010), and with the broad regional uplift along the OBG fault zone (Fig. 8) lowering the vertical stress, northwest–southeast-trending pre-existing structures in the OBG, could potentially be reactivated in a reverse sense. The potential for reactivating the pre-existing structures in the OBG as reverse faults was demonstrated in slip tendency models by Rimando and Peace (2021). Accordingly, neotectonic and paleoseismic studies, including trenching, Quaternary dating, and detailed quantitative slip-rate studies on the OBG fault zone, have the potential to provide vital insights leading to a better understanding of the regional seismic hazards in eastern Canada.

There appears to be a link between relatively high uplift rate locations and the occurrence of the earthquake records. Our findings document the long-term deformation history of the OBG, which may contribute to the ongoing seismicity. For instance, sections 1–3 (Fig. 1) lie very close to the epicentres of the Timiskaming earthquake (1935, Mw 6.1), Ladysmith earthquake (2013, Mw 4.6), and Val-des-Bois earthquake (2010, Mw 5.0), respectively (Figs. 1 and 2) and they also exhibit relatively high uplift rates (Fig. 6). With their northwest–southeast to west northwest–east-southeast striking faults, section 2 down to section 3 near Eardley Faults (fault 3 in Fig. 1) and west northwest–east-southeast striking faults, section 4 near Gatineau Fault (fault 4 in Fig. 1) lie perpendicularly to the present-day maximum horizontal stress (Mazzotti and Townend 2010; Hurd and Zoback 2012). Sections 2–4 have relatively high uplift rates, and also show relatively high slip tendency values according to the results of Rimando and Peace (2021). This area could therefore provide a promising location for conducting future geophysical and paleoseismic investigations to collect fault geometry and kinematic data. The WNW–ESE striking faults in the eastern OBG, from Lachute Fault (fault 5 in Fig. 1) to New Glasgow Fault (fault 6 in Fig. 1), that lie parallel to the seismicity trend and postulated ancient hotspot track (Ma and Eaton 2007), are also optimally oriented with respect to the present-day stress field and may also be good candidates for further detailed investigations. Mapping these structures may be difficult, however, since the faults do not have a strong topographic expression, and the topographic expression of the New Glasgow Fault (fault 6 in Fig. 1) might

have been modified by urbanization as it is located near Montreal.

Furthermore, the Eardley, Gatineau, Lachute, and New Glasgow faults (faults 3–6 in Fig. 1, respectively) coincide spatially with high uplift rate signals, and therefore, may also represent candidate sites for future, more detailed, slip-rate and Quaternary dating studies. The need for site-specific studies in areas exhibiting high relative uplift is corroborated by modelling of potential fault reactivation in the WQSZ by Rimando and Peace (2021). Paleoseismic trenching in the vicinity of these bedrock escarpments which have high relative uplift rates could possibly reveal recent or historical earthquake features. They can also provide further insights on the role of pre-existing structures on the distribution and generation of earthquakes.

While the reactivation of inherited structures is likely the main cause of seismicity in this cratonic low-strain region, identifying and indeed linking possible surface ruptures and their relationship at depth is problematic (Bent and Perry 2002; Bent et al. 2003; Ma and Eaton 2007). In eastern Canada, earthquakes surface ruptures are scarce, with most faults not reaching the surface. This is challenging due to several cycles of glacial retreats that eroded Quaternary deposits and Quaternary faults, which makes the study of earthquake geology problematic. Given the scarcity of surface ruptures, evidence of palaeoseismicity had been identified on quick clay deposits related to landslides in the OBG (Fig. 3) (Brooks 2013, 2020; Doughty et al. 2010a, b). However, in the riverbed of the St. Lawrence River, the relationship between pre-existing structures and displacement of Quaternary sediment above pre-Tertiary bedrock has been identified on bathymetry and seismic profile data (Pinet et al. 2021). Further mapping of pre-existing faults using surface and subsurface methods would be useful to better characterize fault geometry (strike, dip, and length), and to locate Quaternary fault traces. Therefore, areas with moderate to relatively high uplift rates should also be considered in seismic hazard assessment since these can trigger reactivation of pre-existing structures and rejuvenate the landscape.

6. Conclusions

Our morphotectonic investigation of the OBG drainage basins contributes to a record of long-term deformation caused by far-field tectonic stresses that predate GIA, resulting in broad wavelength regional uplift that has probably been active since the Pleistocene. The landscape is still evolving as a result of the reactivation of pre-existing structures, while also undergoing isostasy adjustment as a consequence deglaciation, and the reactivation of pre-existing structures.

This study details the first application of morphotectonic analysis to the OBG bedrock escarpment. The distribution of the high k_{sn} can be observed along high local relief and is located near mapped pre-existing structures. Although, k_{sn} and V_f ratio analysis infer that the relative uplift rates are classified as high, their degree of activity is relatively low to moderate compared to interplate (plate boundary) settings. None of the subcatchments show asymmetric up-

lift patterns, demonstrating the trend of uplift can be inferred as broad wavelength regional uplift. Thus, relatively high local relief, moderate to high k_{sn} values, and basin elongation ratio shows that the OBG experienced uplift since Pleistocene or multiphase uplift before and after last glacial maximum.

This study has established regional relative uplift rates for the OBG. These relative uplift rates from the combination of indices used herein is in agreement with previous GPS studies, demonstrating that they are a powerful tool in quantifying spatial and temporal regional relative uplift rates in regions of relatively low relief and low-to-moderate rates of deformation. As such, interpreting various geomorphic indices together to evaluate rates drainage basin relative uplift rates is more effective than evaluating such indices individually as certain indices may be sensitive to other factors such as climatic variation and glacial erosion.

This study has highlighted structures that should be the focus of future more localized and detailed work, specifically, section 3 near the Eardley Fault (fault 3 in Fig. 1), section 4 near Gatineau Fault (fault 4 in Fig. 1), and section 5 near Lachute Fault and New Glasgow Fault (faults 5 and 6 in Fig. 1, respectively) at the eastern end of OBG, which were characterized in this study as having moderate to high relative uplift rates and also in proximity to the past earthquake epicentres. These sites may reveal evidence of reactivation of pre-existing structures and landscape rejuvenation. They may also represent ideal locations for further quantification of post-Mesozoic deformation (Cenozoic to perhaps Quaternary) that may yield further insights into the causes and consequences of the seismicity in this region.

Acknowledgements

We would like to acknowledge Dr. Wolfgang Schwanghart for assistance with TopoToolBox software, and ESRI for providing a student license to support this research. Two anonymous reviewers are thanked for their constructive input on this manuscript. We would also like to thank Dr. J. Brendan Murphy for handling this manuscript.

Article information

History dates

Received: 9 December 2022

Accepted: 14 February 2023

Accepted manuscript online: 15 February 2023

Version of record online: 16 March 2023

Copyright

© 2023 The Author(s). Permission for reuse (free in most cases) can be obtained from [copyright.com](https://www.copyright.com).

Data availability

Data generated or analysed during this study are available from the corresponding author upon reasonable request.

Author information

Author ORCIDs

Ugi K. Gusti <https://orcid.org/0000-0003-4890-815X>

Alexander L. Peace <https://orcid.org/0000-0001-7846-3898>

Jeremy Rimando <https://orcid.org/0000-0003-2437-4579>

Author contributions

Conceptualization: UKG, ALP, JR

Data curation: UKG

Formal analysis: UKG, JR

Funding acquisition: ALP

Investigation: UKG, ALP, JR

Methodology: UKG, JR

Project administration: UKG

Resources: ALP

Supervision: ALP, JR

Validation: UKG, ALP, JR

Visualization: UKG, ALP, JR

Writing – original draft: UKG

Writing – review & editing: UKG, ALP, JR

Competing interests

The authors declare there are no competing interests.

Funding information

Ugi Kurnia Gusti was funded to undertake this work through a Ph.D. studentship in the School of Earth, Environment, and Society, McMaster University. Jeremy Rimando's Postdoctoral Fellowship was funded in part by the Keith Macdonald structural geology advancement fund, and the NSERC-Alliance grant (ALLRP 567023-21) to Katsu Goda, Alexander Peace, and Luc Chouinard in partnership with the Institute of Catastrophic Loss Reduction (ICLR). Alexander Peace also acknowledges NSERC Discovery Grant RGPIN-2021-04011 for support of his research program which partially supported Ugi Kurnia Gusti's Ph.D. studentship.

Supplementary material

Supplementary data are available with the article at <https://doi.org/10.1139/cjes-2022-0137>.

References

- Adams, J. 1989. Postglacial faulting in eastern Canada: nature, origin and seismic hazard implications. *Tectonophysics*, **163**: 323–331. doi:10.1016/0040-1951(89)90267-9.
- Adams, J. 2011. Seismic hazard maps for the National Building Code of Canada. In *Proceedings, Annual Conference – Canadian Society for Civil Engineering*. pp. 896–905.
- Adams, J., and Basham, P. 1989. The seismicity and seismotectonics of Canada east of the Cordillera. *Geoscience Canada*, **16**: 3–16.
- Alinia, H.S., Tiampo, K.F., and James, T.S. 2017. GPS coordinate time series measurements in Ontario and Quebec, Canada. *Journal of Geodesy*, **91**: 653–683. doi:10.1007/s00190-016-0987-5.
- Baharvand, S., Pardhan, B., and Soori, S. 2020. Evaluation of active tectonics using geomorphic indices in a mountainous basin of Iran. *Earth and Environmental Science Transactions of the Royal Society of Edinburgh*, **111**: 109–117. doi:10.1017/S1755691020000031.
- Baird, A.F., McKinnon, S.D., and Godin, L. 2010. Relationship between structures, stress and seismicity in the Charlevoix seismic zone revealed by 3-D geomechanical models: implications for the seismotectonics of continental interiors. *Journal of Geophysical Research*, **115**: 1–16. doi:10.1029/2010JB007521.
- Bent, A.L. 1996a. An improved source mechanism for the 1935 Timiskaming, Quebec earthquake from regional waveforms. *Pure and Applied Geophysics*, **146**: 5–20. Birkhauser Verlag AG. doi:10.1007/bf00876667.
- Bent, A.L., and Perry, H.K.C. 2002. Depths of eastern Canadian earthquakes from regional data. *Seismological Research Letters*, **73**: 273–284. Seismological Society of America. doi:10.1785/gssrl.73.2.273.
- Bent, A.L., Drysdale, J., and Perry, H.K.C. 2003. Focal mechanisms for Eastern Canadian Earthquakes, 1994–2000. *Seismological Research Letters*, **74**: 452–468. Seismological Society of America. doi:10.1785/gssrl.74.4.452.
- Bent, A.L., Lamontagne, M., Adams, J., Woodgoid, C.R.D., Haichuk, S., Drysdale, J., et al. 2002. The Kipawa, Quebec “millennium” earthquake. *Seismological Research Letters*, **73**: 285–297. doi:10.1785/gssrl.73.2.285.
- Bent, A.L., Lamontagne, M., Peci, V., Halchuk, S., Brooks, G.R., Motazedian, D., et al. 2015. The 17 May 2013 M 4.6 Ladysmith, Quebec, earthquake. *Seismological Research Letters*, **86**: 460–476. doi:10.1785/0220140138.
- Bookhagen, B., and Strecker, M.R. 2012. Spatiotemporal trends in erosion rates across a pronounced rainfall gradient: examples from the southern Central Andes. *Earth and Planetary Science Letters*, **327**–**328**: 97–110. Elsevier. doi:10.1016/j.epsl.2012.02.005.
- Boulton, S.J. 2020. Geomorphic response to differential uplift: river long profiles and knickpoints from Guadalcanal and Makira (Solomon Islands). *Frontiers in Earth Science*, **8**. doi:10.3389/feart.2020.00010.
- Brocklehurst, S.H., and Whipple, K.X. 2007. Response of glacial landscapes to spatial variations in rock uplift rate. *Journal of Geophysical Research*, **112**. Blackwell Publishing Ltd. doi:10.1029/2006JF000667.
- Brooks, G.R. 2013. A massive sensitive clay landslide, Quyon Valley, southwestern Quebec, Canada, and evidence for a paleoearthquake triggering mechanism. *Quaternary Research*, **80**: 425–434. Elsevier B.V. doi:10.1016/j.yqres.2013.07.008.
- Brooks, G.R. 2020. Evidence of a strong paleoearthquake in ~9.1 ka cal BP interpreted from mass transport deposits, western Quebec – north-eastern Ontario, Canada. *Quaternary Science Reviews*, **234**: 106250. Elsevier Ltd. doi:10.1016/j.quascirev.2020.106250.
- Brooks, G.R., and Adams, J. 2020. A review of evidence of glacially-induced faulting and seismic shaking in eastern Canada. *Quaternary Science Reviews*, **228**: 106070. Elsevier Ltd. doi:10.1016/j.quascirev.2019.106070.
- Bucci, M.G., and Schoenbohm, L.M. 2022. Tectono-geomorphic analysis in low relief, low tectonic activity areas: case study of the Temiskaming Region in the Western Quebec Seismic Zone (WQSZ), Eastern Canada. *Remote Sensing*, **14**: 3587. Multidisciplinary Digital Publishing Institute. doi:10.3390/RS14153587.
- Bull, W. 2008. *Tectonic geomorphology of mountains: a new approach to paleoseismology*. John Wiley & Sons.
- Bull, W.B., and McFadden, L.D. 1977. Tectonic geomorphology north and south of the Garlock fault, California. In *Geomorphology in arid regions. Proceedings of 8th Binghamton Symposium in Geomorphology*, Routledge. pp. 115–138. doi:10.4324/9780429299230-5.
- Calais, E., Camelbeeck, T., Stein, S., Liu, M., and Craig, T.J. 2016. A new paradigm for large earthquakes in stable continental plate interiors. *Geophysical Research Letters*, **43**: 10621–10637. doi:10.1002/2016GL070815.
- Cannon, P. 1977. Generation of explicit parameters for a quantitative geomorphic study of the Mill creek drainage basin. *Oklahoma Geology Notes*, **36**: 3–16.
- Carson, M., and Kirkby, M. 1972. *Hillslope form and process*. Cambridge University Press, New York, 476 pp.
- Chen, Y.-C., Sung, Q., and Cheng, K.-Y. 2003. Along-strike variations of morphotectonic features in the Western Foothills of Taiwan: tectonic implications based on stream-gradient and hypsometric analysis. *Geomorphology*, **56**: 109–137. Elsevier. doi:10.1016/S0169-555X(03)00059-X.
- Cheng, Y., He, C., Rao, G., Yan, B., Lin, A., Hu, J., et al. 2018. Geomorphological and structural characterization of the southern Weihe Graben, central China: implications for fault segmentation. *Tectonophysics*, **722**: 11–24. Elsevier. doi:10.1016/j.tecto.2017.10.024.

- Chorley, R.J., and K. 1971. *Chorley: physical geography: a systems approach*. Prentice-Hall.
- Clayton, K., and Shamoon, N. 1998. A new approach to the relief of Great Britain II. A classification of rocks based on relative resistance to denudation. *Geomorphology*, **25**: 155–171. Elsevier. doi:[10.1016/S0169-555X\(98\)00038-5](https://doi.org/10.1016/S0169-555X(98)00038-5).
- Cyr, A.J., Granger, D.E., Olivetti, V., and Molin, P. 2010. Quantifying rock uplift rates using channel steepness and cosmogenic nuclide-determined erosion rates: examples from northern and southern Italy. *Lithosphere*, **2**: 188–198. Geological Society of America. doi:[10.1130/L96.1](https://doi.org/10.1130/L96.1).
- DiBiase, R.A., Whipple, K.X., Heimsath, A.M., and Ouimet, W.B. 2010. Landscape form and millennial erosion rates in the San Gabriel Mountains, CA. *Earth and Planetary Science Letters*, **289**: 134–144. Elsevier. doi:[10.1016/j.epsl.2009.10.036](https://doi.org/10.1016/j.epsl.2009.10.036).
- Dickin, A., Strong, J., Arcuri, G., Van Kessel, A., and Krivankova-Smal, L. 2017. A revised model for the crustal structure of the SW Grenville Province, Ontario, Canada. *Geological Magazine*, **154**: 903–913. Cambridge University Press. doi:[10.1017/S001675681700005X](https://doi.org/10.1017/S001675681700005X).
- Dickin, A.P., and Guo, A. 2001. The location of the Allochthon Boundary Thrust and the Archean-Proterozoic suture in the Mattawa area of the Grenville Province: Nd isotope evidence. *Precambrian Research*, **107**: 31–43. Elsevier. doi:[10.1016/S0301-9268\(00\)00153-4](https://doi.org/10.1016/S0301-9268(00)00153-4).
- Dineva, S., Eaton, D., Ma, S., and Mereu, R. 2007. The October 2005 Georgian Bay, Canada, Earthquake Sequence: Mafic Dykes and their role in the mechanical heterogeneity of Precambrian Crust. *Bulletin of the Seismological Society of America*, **97**: 457–473. GeoScienceWorld. doi:[10.1785/0120060176](https://doi.org/10.1785/0120060176).
- Doughty, M., Eyles, N., and Daurio, L. 2010a. Earthquake-triggered slumps (1935 Timiskaming M6.2) in Lake Kipawa, Western Quebec Seismic Zone, Canada. *Sedimentary Geology*, **228**: 113–118. Elsevier B.V. doi:[10.1016/j.sedgeo.2010.04.003](https://doi.org/10.1016/j.sedgeo.2010.04.003).
- Doughty, M., Eyles, N., and Daurio, L. 2010b. Ongoing neotectonic activity in the Timiskaming - Kipawa area of Ontario and Québec. *Geoscience Canada*, **37**: 109–116. Available from <https://journals.lib.unb.ca/index.php/GC/article/view/18397/19865> [accessed 24 November 2022].
- Du, W.X., Kim, W.Y., and Sykes, L.R. 2003. Earthquake source parameters and state of stress for the Northeastern United States and Southeastern Canada from analysis of regional seismograms. *Bulletin of the Seismological Society of America*, **93**: 1633–1648. GeoScienceWorld. doi:[10.1785/0120020217](https://doi.org/10.1785/0120020217).
- Duvall, A. 2004. Tectonic and lithologic controls on bedrock channel profiles and processes in coastal California. *Journal of Geophysical Research*, **109**: F03002. American Geophysical Union (AGU). doi:[10.1029/2003JF000086](https://doi.org/10.1029/2003JF000086).
- Dyke, A.S., Andrews, J.T., Clark, P.U., England, J.H., Miller, G.H., Shaw, J., and Veillette, J.J. 2002. The Laurentide and Innuitian ice sheets during the Last Glacial Maximum. *Quaternary Science Reviews*, **21**: 9–31. Pergamon. doi:[10.1016/S0277-3791\(01\)00095-6](https://doi.org/10.1016/S0277-3791(01)00095-6).
- El Hamdouni, R., Irigaray, C., Fernández, T., Chacón, J., and Keller, E.A. 2008. Assessment of relative active tectonics, southwest border of the Sierra Nevada (southern Spain). *Geomorphology*, **96**: 150–173. Elsevier. doi:[10.1016/j.geomorph.2007.08.004](https://doi.org/10.1016/j.geomorph.2007.08.004).
- Elliott, J.R., Copley, A.C., Holley, R., Scharer, K., and Parsons, B. 2013. The 2011 Mw 7.1 Van (Eastern Turkey) earthquake. *Journal of Geophysical Research: Solid Earth*, **118**: 1619–1637. John Wiley & Sons, Ltd. doi:[10.1002/JGRB.50117](https://doi.org/10.1002/JGRB.50117).
- Fielding, E.J., Lundgren, P.R., Taymaz, T., Yolsal-Çevikbilen, S., and Owen, S.E. 2013a. Fault-Slip Source Models for the 2011 M 7.1 Van Earthquake in Turkey from SAR Interferometry, Pixel Offset Tracking, GPS, and Seismic Waveform Analysis. *Seismological Research Letters*, **84**: 579–593. GeoScienceWorld. doi:[10.1785/0220120164](https://doi.org/10.1785/0220120164).
- Fielding, E.J., Sladen, A., Li, Z., Avouac, J.-P., Bürgmann, R., and Ryder, I. 2013b. Kinematic fault slip evolution source models of the 2008 M7.9 Wenchuan earthquake in China from SAR interferometry, GPS and teleseismic analysis and implications for Longmen Shan tectonics. *Geophysical Journal International*, **194**: 1138–1166. Oxford Academic. doi:[10.1093/GJI/JGGT155](https://doi.org/10.1093/GJI/JGGT155).
- Gailleton, B., Sinclair, H.D., Mudd, S.M., Graf, E.L.S., and Maçenco, L.C. 2021. Isolating lithologic versus tectonic signals of river profiles to test orogenic models for the Eastern and Southeastern Carpathians. *Journal of Geophysical Research: Earth Surface*, **126**: 1–26. doi:[10.1029/2020JF005970](https://doi.org/10.1029/2020JF005970).
- Goda, K. 2019a. Nationwide earthquake risk model for wood-frame houses in Canada. *Frontiers in Built Environment*, **5**: 128. Frontiers. doi:[10.3389/FBUIL.2019.00128](https://doi.org/10.3389/FBUIL.2019.00128).
- Gold, R.D., Clark, D., Barnhart, W.D., King, T., Quigley, M., and Briggs, R.W. 2019. Surface rupture and distributed deformation revealed by optical satellite imagery: The Intraplate 2016 Mw 6.0 Petermann Ranges Earthquake, Australia. *Geophysical Research Letters*, **46**: 10394–10403. John Wiley & Sons, Ltd. doi:[10.1029/2019GL084926](https://doi.org/10.1029/2019GL084926).
- Guo, A., and Dickin, A.P. 1996. The southern limit of Archean crust and significance of rocks with Paleoproterozoic model ages: Nd model age mapping in the Grenville Province of western Quebec. *Precambrian Research*, **77**: 231–241. Elsevier. doi:[10.1016/0301-9268\(95\)00095-X](https://doi.org/10.1016/0301-9268(95)00095-X).
- Hack, J.T. 1973. Stream-profile analysis and stream-gradient index. *Journal of Research of the U.S. Geological Survey*, **1**: 499.
- Hatcher, R.D. 2010. The Appalachian orogen: a brief summary. *Memoir of the Geological Society of America*, **206**: 1–19. Geological Society of America. doi:[10.1130/2010.1206\(01\)](https://doi.org/10.1130/2010.1206(01)).
- Henton, J.A., Craymer, M.R., Ferland, R., Dragert, H., Mazzotti, S., and Forbes, D.L. 2006. Crustal motion and deformation monitoring of the Canadian landmass. *Geomatica*, **60**: 173–191. doi:[10.5623/geomat-2006-0021](https://doi.org/10.5623/geomat-2006-0021).
- Hurd, O., and Zoback, M.D. 2012. Intraplate earthquakes, regional stress and fault mechanics in the central and eastern U.S. and Southeastern Canada. *Tectonophysics*, **581**: 182–192. Elsevier B.V. doi:[10.1016/j.tecto.2012.04.002](https://doi.org/10.1016/j.tecto.2012.04.002).
- International Seismological Centre 2021. On-line Bulletin. Available from <https://doi.org/10.31905/D808B830>.
- Jansen, J.D., Codilean, A.T., Bishop, P., and Hoey, T.B. 2010. Scale dependence of lithological control on topography: bedrock channel geometry and catchment morphometry in Western Scotland. *The Journal of Geology*, **118**: 223–246. The University of Chicago Press. doi:[10.1086/651273](https://doi.org/10.1086/651273).
- Jobe, J.A.T., Gold, R.D., Briggs, R.W., Williams, R.A., Stephenson, W.J., Delano, J.E., et al. 2020. Evidence for late quaternary deformation along Crowleys Ridge, New Madrid Seismic Zone. *Tectonics*, **39**: 0–3. doi:[10.1029/2019TC005746](https://doi.org/10.1029/2019TC005746).
- Jobe, J.T., Hatem, A., Gold, R., DuRoss, C., Reitman, N., Briggs, R., and Collett, C. 2022. Revised earthquake geology inputs for the Central and Eastern United States and Southeast Canada for the 2023 National Seismic Hazard Model. *Seismological Research Letters*, **93**: 3100–3120. GeoScienceWorld. doi:[10.1785/0220220162](https://doi.org/10.1785/0220220162).
- Karlstrom, K.E., Åhäll, K.I., Harlan, S.S., Williams, M.L., McLelland, J., and Geissman, J.W. 2001. Long-lived (1.8–1.0 Ga) convergent orogen in southern Laurentia, its extensions to Australia and Baltica, and implications for refining Rodinia. *Precambrian Research*, **111**: 5–30. doi:[10.1016/S0301-9268\(01\)00154-1](https://doi.org/10.1016/S0301-9268(01)00154-1).
- Keller, E.A., and Pinter, N. 1987. *Active tectonics: earthquakes, uplift, and landscape*. Eos Transactions. Prentice Hall, Upper Saddle River, NJ. pp. AGU68164. doi:[10.1029/eo0681012p00164-02](https://doi.org/10.1029/eo0681012p00164-02).
- King, T.R., Quigley, M., Clark, D., Zondervan, A., May, J.-H., and Alimanovic, A. 2021. Paleoseismology of the 2016 M W 6.1 Petermann earthquake source: implications for intraplate earthquake behaviour and the geomorphic longevity of bedrock fault scarps in a low strain-rate cratonic region. *Earth Surface and Processes Landforms*, **46**: 1238–1256. John Wiley & Sons, Ltd. doi:[10.1002/esp.5090](https://doi.org/10.1002/esp.5090).
- Kirby, E., and Whipple, K.X. 2012. Expression of active tectonics in erosional landscapes. *Journal of Structural Geology*, **44**: 4454. Pergamon. doi:[10.1016/j.jsg.2012.07.009](https://doi.org/10.1016/j.jsg.2012.07.009).
- Kirby, E., Whipple, K., and Harkins, N. 2008. Topography reveals seismic hazard. *Nature Geoscience*, **1**: 1485. Nature Publishing Group. doi:[10.1038/ngeo265](https://doi.org/10.1038/ngeo265).
- Kirby, E., Whipple, K.X., Tang, W., and Chen, Z. 2003. Distribution of active rock uplift along the eastern margin of the Tibetan Plateau: Inferences from bedrock channel longitudinal profiles. *Journal of Geophysical Research*, **108**: 2217. American Geophysical Union (AGU). doi:[10.1029/2001JB000861](https://doi.org/10.1029/2001JB000861).
- Kober, L. 1928. *Der Bau der Erde*. 2nd ed, Borntraeger, Berlin.
- Korup, O. 2008. Rock type leaves topographic signature in landslide-dominated mountain ranges. *Geophysical Research Letters*, **35**. John Wiley & Sons, Ltd. doi:[10.1029/2008GL034157](https://doi.org/10.1029/2008GL034157).
- Krystowicz, N.J., Schoenbohm, L.M., Rimando, J., Brocard, G., and Rojay, B. 2020. Tectonic geomorphology and Plio-Quaternary structural evolution of the Tuzgölü fault zone, Turkey: implications for defor-

- mation in the interior of the Central Anatolian Plateau. *Geosphere*, **16**: 1107–1124. doi:[10.1130/GES02175.1](https://doi.org/10.1130/GES02175.1).
- Kühni, A., and Pfiffner, O.A. 2001. The relief of the Swiss Alps and adjacent areas and its relation to lithology and structure: topographic analysis from a 250-m DEM. *Geomorphology*, **41**: 285–307. Elsevier. doi:[10.1016/S0169-555X\(01\)00060-5](https://doi.org/10.1016/S0169-555X(01)00060-5).
- Kumarapeli, P.S. 1978. The St. Lawrence Paleo-Rift system: a comparative study. In *Tectonics and Geophysics of Continental Rifts*. Springer Netherlands, Dordrecht. pp. 367–384. doi:[10.1007/978-94-009-9806-3_29](https://doi.org/10.1007/978-94-009-9806-3_29).
- Lamontagne, M., and Ranalli, G. 1996. Thermal and rheological constraints on the earthquake depth distribution in the Charlevoix, Canada, intraplate seismic zone. *Tectonophysics*, **257**: 55–69. Elsevier. doi:[10.1016/0040-1951\(95\)00120-4](https://doi.org/10.1016/0040-1951(95)00120-4).
- Lamontagne, M., Brouillette, P., Grégoire, S., Bédard, M.P., and Bleeker, W. 2020. Faults and lineaments of the Western Quebec Seismic Zone, Quebec and Ontario, Geological Survey of Canada, Open File 8361, 2020, 28 pages (1 sheet) [10.4095/321900](https://doi.org/10.4095/321900).
- Lamontagne, M., Keating, P., and Perreault, S. 2003. Seismotectonic characteristics of the lower St. Lawrence seismic zone, Quebec: insights from geology, magnetism, gravity, and seismics. *Canadian Journal of Earth Sciences*, **40**: 317–336. doi:[10.1139/e02-104](https://doi.org/10.1139/e02-104).
- Lemieux, Y., Tremblay, A., and Lavoie, D. 2003. Structural analysis of supracrustal faults in the Charlevoix area, Quebec: relation to impact cratering and the St-Laurent fault system 1. doi:[10.1139/E02-046](https://doi.org/10.1139/E02-046).
- Lifton, N.A., and Chase, C.G. 1992. Tectonic, climatic and lithologic influences on landscape fractal dimension and hypsometry: implications for landscape evolution in the San Gabriel Mountains, California. *Geomorphology*, **5**: 77–114. Elsevier. doi:[10.1016/0169-555X\(92\)90059-W](https://doi.org/10.1016/0169-555X(92)90059-W).
- Ma, S., and Eaton, D.W. 2007. Western Quebec seismic zone (Canada): clustered, midcrustal seismicity along a Mesozoic hot spot track. *Journal of Geophysical Research*, **112**. John Wiley & Sons, Ltd. doi:[10.1029/2006JB004827](https://doi.org/10.1029/2006JB004827).
- Ma, S., and Motazedian, D. 2012. Studies on the June 23, 2010 north Ottawa M_W 5.2 earthquake and vicinity seismicity. *Journal of Seismology*, **16**: 513–534. doi:[10.1007/s10950-012-9294-7](https://doi.org/10.1007/s10950-012-9294-7).
- Ma, S., Eaton, D.W., and Adams, J. 2008. Intraplate seismicity of a recently deglaciated shield terrane: a case study from Northern Ontario, Canada. *Bulletin of the Seismological Society of America*, **98**: 2828–2848. doi:[10.1785/0120080134](https://doi.org/10.1785/0120080134).
- Marliyani, G.I., Arrowsmith, J.R., and Whipple, K.X. 2016. Characterization of slow slip rate faults in humid areas: Cimandiri fault zone, Indonesia. *Journal of Geophysical Research: Earth Surface*, **121**: 2287–2308. doi:[10.1002/2016JF003846](https://doi.org/10.1002/2016JF003846).
- Mathew, M.J., Menier, D., Siddiqui, N., Kumar, S.G., and Authemayou, C. 2016a. Active tectonic deformation along rejuvenated faults in tropical Borneo: Inferences obtained from tectono-geomorphic evaluation. *Geomorphology*, **267**: 1–15. Elsevier B.V. doi:[10.1016/j.geomorph.2016.05.016](https://doi.org/10.1016/j.geomorph.2016.05.016).
- Mathew, M.J., Menier, D., Siddiqui, N., Ramkumar, M., Santosh, M., Kumar, S., and Hassaan, M. 2016b. Drainage basin and topographic analysis of a tropical landscape: Insights into surface and tectonic processes in northern Borneo. *Journal of Asian Earth Sciences*, **124**: 14–27. Elsevier Ltd. doi:[10.1016/j.jseaes.2016.04.016](https://doi.org/10.1016/j.jseaes.2016.04.016).
- Mazzotti, S., and Gueydan, F. 2018. Control of tectonic inheritance on continental intraplate strain rate and seismicity. *Tectonophysics*, **746**: 602–610. Elsevier. doi:[10.1016/j.tecto.2017.12.014](https://doi.org/10.1016/j.tecto.2017.12.014).
- Mazzotti, S., and Townend, J. 2010. State of stress in central and eastern North American seismic zones. *Lithosphere*, **2**: 76–83. doi:[10.1130/L65.1](https://doi.org/10.1130/L65.1).
- Mazzotti, S., James, T.S., Henton, J., and Adams, J. 2005. GPS crustal strain, postglacial rebound, and seismic hazard in eastern North America: The Saint Lawrence valley example. *Journal of Geophysical Research*, **110**: 1–16. doi:[10.1029/2004JB003590](https://doi.org/10.1029/2004JB003590).
- Mezger, K., Essene, E.J., van der Pluijm, B.A., and Halliday, A.N. 1993. U-Pb geochronology of the Grenville Orogen of Ontario and New York: constraints on ancient crustal tectonics. *Contributions to Mineralogy and Petrology*, **114**: 13–26. Springer. doi:[10.1007/BF00307862](https://doi.org/10.1007/BF00307862).
- Mohajer, E., Eyles, N., and Rogojina, C. 1992. Neotectonic faulting in metropolitan Toronto: implications for earthquake hazard assessment in the Lake Ontario region. *Geology*, **20**: 1003. doi:[10.1130/0091-7613\(1992\)020\(1003:NFMIT\)2.3.CO;2](https://doi.org/10.1130/0091-7613(1992)020(1003:NFMIT)2.3.CO;2).
- Mudd, S.M., Clubb, F.J., Gailleton, B., and Hurst, M.D. 2018. How concave are river channels? *Earth Surface Dynamics*, **6**: 505–523. doi:[10.5194/esurf-6-505-2018](https://doi.org/10.5194/esurf-6-505-2018).
- NASA/METI/AIST/Japan Space Systems and U.S./Japan ASTER Science Team. 2019. Aster Global Digital Elevation Model V003. doi:[10.5067/ASTER/ASTGTM.003](https://doi.org/10.5067/ASTER/ASTGTM.003).
- NRCC. 2010. National Building Code of Canada. Government of Canada, **1**: 1222.
- Ntokos, D., Lykoudi, E., and Rondoyanni, T. 2016. Geomorphic analysis in areas of low-rate neotectonic deformation: South Epirus (Greece) as a case study. *Geomorphology*, **263**: 156–169. Elsevier B.V. doi:[10.1016/j.geomorph.2016.04.005](https://doi.org/10.1016/j.geomorph.2016.04.005).
- Ojo, A.O., Kao, H., Jiang, Y., Craymer, M., and Henton, J. 2021. Strain accumulation and release rate in Canada: implications for long-term crustal deformation and earthquake hazards. *Journal of Geophysical Research*, **126**: e2020JB020529. John Wiley & Sons, Ltd. doi:[10.1029/2020JB020529](https://doi.org/10.1029/2020JB020529).
- Oruche, N.E., Dix, G.R., and Kamo, S.L. 2018. Lithostratigraphy of the upper Turinian – lower Chatfieldian (Upper Ordovician) foreland succession, and a U-Pb ID-TIMS date for the Millbrig volcanic ash bed in the Ottawa Embayment. *Canadian Journal of Earth Sciences*, **55**: 1079–1102. GeoScienceWorld. doi:[10.1139/CJES-2018-0006](https://doi.org/10.1139/CJES-2018-0006).
- Peace, A.L., Phethean, J.J., Franke, D., Foulger, G.R., Schiffer, C., Welford, J.K., et al. 2020. A review of Pangaea dispersal and Large Igneous Provinces – In search of a causative mechanism. *Earth-Science Reviews*, **206**: 102902. Elsevier. doi:[10.1016/j.earscirev.2019.102902](https://doi.org/10.1016/j.earscirev.2019.102902).
- Pérez-Peña, J. V., Azañón, J.M., and Azor, A. 2009. CalHypso: an ArcGIS extension to calculate hypsometric curves and their statistical moments. Applications to drainage basin analysis in SE Spain. *Computers & Geosciences*, **35**: 1214–1223. Pergamon. doi:[10.1016/j.cageo.2008.06.006](https://doi.org/10.1016/j.cageo.2008.06.006).
- Pinet, N., Lamontagne, M., Duchesne, M.J., and Brake, V.I. 2021. Hunting for quaternary faults in Eastern Canada: a critical appraisal of two potential candidates. *Seismological Research Letters*, **92**: 1102–1111. doi:[10.1785/0220200322](https://doi.org/10.1785/0220200322).
- Radaideh, O.M.A., Grasemann, B., Melichar, R., and Mosar, J. 2016. Detection and analysis of morphotectonic features utilizing satellite remote sensing and GIS: an example in SW. *Geomorphology*, **275**: 58–79. Elsevier B.V. doi:[10.1016/j.geomorph.2016.09.033](https://doi.org/10.1016/j.geomorph.2016.09.033).
- Ramírez-Herrera, M.T. 1998. Geomorphic assessment of active tectonics in the Acambay Graben, Mexican volcanic belt. *Earth Surface Processes and Landforms*, **23**: 317–332. John Wiley and Sons Ltd. doi:[10.1002/\(SICI\)1096-9837\(199804\)23:4\(317::AID-ESP845\)3.0.CO;2-V](https://doi.org/10.1002/(SICI)1096-9837(199804)23:4(317::AID-ESP845)3.0.CO;2-V).
- Rankin, D.W. 1976. Appalachian salients and recesses: late Precambrian continental breakup and the opening of the Iapetus Ocean. *Journal of Geophysical Research*, **81**: 5605–5619. John Wiley & Sons, Ltd. doi:[10.1029/JB081I032P05605](https://doi.org/10.1029/JB081I032P05605).
- Rimando, J.M., and Peace, A.L. 2021. Reactivation potential of intraplate faults in the Western Quebec Seismic Zone, Eastern Canada. *Earth and Space Science*, **8**: e2021EA001825. John Wiley & Sons, Ltd. doi:[10.1029/2021EA001825](https://doi.org/10.1029/2021EA001825).
- Rimando, J.M., and Schoenbohm, L.M. 2020. Regional relative tectonic activity of structures in the Pampean flat slab segment of Argentina from 30 to 32° S. *Geomorphology*, **350**: 106908. Elsevier B.V. doi:[10.1016/j.geomorph.2019.106908](https://doi.org/10.1016/j.geomorph.2019.106908).
- Rimando, J.M., Schoenbohm, L.M., Ortiz, G., Alvarado, P., Venerdini, A., Owen, L.A., et al. 2021. Late quaternary intraplate deformation defined by the Las Chacras Fault Zone, West-Central Argentina. *Tectonics*, **40**: e2020TC006509. John Wiley & Sons, Ltd. doi:[10.1029/2020TC006509](https://doi.org/10.1029/2020TC006509).
- Rimando, R.E., and Benn, K. 2005. Evolution of faulting and paleo-stress field within the Ottawa graben. *Journal of Geodynamics*, **39**: 337–360. doi:[10.1016/j.jog.2005.01.003](https://doi.org/10.1016/j.jog.2005.01.003).
- Robl, J., Heberer, B., Prasicek, G., Neubauer, F., and Hergarten, S. 2017. The topography of a continental indenter: The interplay between crustal deformation, erosion, and base level changes in the eastern Southern Alps. *Journal of Geophysical Research: Earth Surface*, **122**: 310–334. Blackwell Publishing Ltd. doi:[10.1002/2016JF003884](https://doi.org/10.1002/2016JF003884).
- Rockwell, T.K., and Keller, E.A. 1985. Tectonic geomorphology of alluvial fans and mountain fronts near Ventura, California. In *Tectonic geomorphology. Proceedings of the 15th Annual Geomorphology Symposium*. Allen and Unwin Publishers, Boston, MA. pp. 183–207.

- Russell, H.A.J., Brooks, G.R., and Cummings, D.I. 2011. Deglacial history of the Champlain Sea basin and implications for urbanization. Geological Survey of Canada, Open File, **6947**: 1–96. doi:[10.4095/289555](https://doi.org/10.4095/289555).
- Saber, R., Isik, V., and Caglayan, A. 2020. Tectonic geomorphology of the Aras drainage basin (NW Iran): implications for the recent activity of the Aras fault zone. Geological Journal, **55**: 5022–5048. John Wiley & Sons, Ltd. doi:[10.1002/GJ.3724](https://doi.org/10.1002/GJ.3724).
- Sanford, B.V. 1993. St. Lawrence Platform—geology. In Sedimentary cover of the Craton in Canada. Geological Society of America. pp. 723–786. doi:[10.1130/DNAG-GNA-D1.723](https://doi.org/10.1130/DNAG-GNA-D1.723).
- Schiffer, C., Doré, A.G., Foulger, G.R., Franke, D., Geoffroy, L., Gernigon, L., et al. 2020. Structural inheritance in the North Atlantic. Earth-Science Reviews, **206**: 102975. Elsevier. doi:[10.1016/j.EARSCIREV.2019.102975](https://doi.org/10.1016/j.EARSCIREV.2019.102975).
- Schumm, S.A. 1956. Evolution of drainage systems and slopes in badlands at Perth Amboy, New Jersey. Geological Society of America Bulletin, **67**: 597–646. GeoScienceWorld. doi:[10.1130/0016-7606\(1956\)67\[597:EODSAS\]2.0.CO;2](https://doi.org/10.1130/0016-7606(1956)67[597:EODSAS]2.0.CO;2).
- Schwanghart, W., and Scherler, D. 2014. Short Communication: TopoToolbox 2 - MATLAB-based software for topographic analysis and modeling in Earth surface sciences. Earth Surface Dynamics, **2**: 1–7. Copernicus GmbH. doi:[10.5194/esurf-2-1-2014](https://doi.org/10.5194/esurf-2-1-2014).
- Selby, M.J. 1980. A rock mass strength classification for geomorphic purposes: with tests from Antarctica and New Zealand. Zeitschrift für Geomorphologie, **24**: 31–51. doi:[10.1127/zfg/24/1984/31](https://doi.org/10.1127/zfg/24/1984/31).
- Sella, G.F., Stein, S., Dixon, T.H., Craymer, M., James, T.S., Mazzotti, S., and Dokka, R.K. 2007. Observation of glacial isostatic adjustment in “stable” North America with GPS. Geophysical Research Letters, **34**: L02306. doi:[10.1029/2006GL027081](https://doi.org/10.1029/2006GL027081).
- Snyder, N.P., Whipple, K.X., Tucker, G.E., and Merritts, D.J. 2000. Landscape response to tectonic forcing: digital elevation model analysis of stream profiles in the Mendocino triple junction region, Northern California. Bulletin of the Geological Society of America, **112**: 1250–1263. Geological Society of America. doi:[10.1130/0016-7606\(2000\)112\(1250:LRTTFD\)2.0.CO;2](https://doi.org/10.1130/0016-7606(2000)112(1250:LRTTFD)2.0.CO;2).
- Steffen, R., Eaton, D.W., and Wu, P. 2012. Moment tensors, state of stress and their relation to post-glacial rebound in northeastern Canada. Geophysical Journal International, **189**: 1741–1752. doi:[10.1111/j.1365-246X.2012.05452.x](https://doi.org/10.1111/j.1365-246X.2012.05452.x).
- Stephenson, R., Schiffer, C., Peace, A., Nielsen, S.B., and Jess, S. 2020. Late Cretaceous-Cenozoic basin inversion and palaeostress fields in the North Atlantic-western Alpine-Tethys realm: implications for intraplate tectonics. Earth-Science Reviews, **210**: 103252. Elsevier. doi:[10.1016/j.EARSCIREV.2020.103252](https://doi.org/10.1016/j.EARSCIREV.2020.103252).
- Sternai, P., Herman, F., Fox, M.R., and Castelltort, S. 2011. Hypsometric analysis to identify spatially variable glacial erosion. Journal of Geophysical Research, **116**: 3001. John Wiley & Sons, Ltd. doi:[10.1029/2010JF001823](https://doi.org/10.1029/2010JF001823).
- Strahler, A.N. 1952. Hypsometric (area-altitude) analysis of erosional topography. Geological Society of America Bulletin, **63**: 1117–1142. GeoScienceWorld. doi:[10.1130/0016-7606\(1952\)63\[1117:HAAOET\]2.0.CO;2](https://doi.org/10.1130/0016-7606(1952)63[1117:HAAOET]2.0.CO;2).
- Tarayoun, A., Mazzotti, S., Craymer, M., and Henton, J. 2018. Structural inheritance control on intraplate present-day deformation: GPS strain rate variations in the Saint Lawrence Valley, Eastern Canada. Journal of Geophysical Research, Solid Earth, **123**: 7004–7020. doi:[10.1029/2017JB015417](https://doi.org/10.1029/2017JB015417).
- Telbisz, T., Kovács, G., Székely, B., and Szabó, J. 2013. Topographic swath profile analysis: a generalization and sensitivity evaluation of a digital terrain analysis tool. Zeitschrift für Geomorphologie, **57**: 485–513. doi:[10.1127/0372-8854/2013/0110](https://doi.org/10.1127/0372-8854/2013/0110).
- Tremblay, A., Long, B., and Massé, M. 2003. Supracrustal faults of the St. Lawrence rift system, Québec: kinematics and geometry as revealed by field mapping and marine seismic reflection data. Tectonophysics, **369**: 231–252. doi:[10.1016/S0040-1951\(03\)00227-0](https://doi.org/10.1016/S0040-1951(03)00227-0).
- Tucker, G.E. 2004. Drainage basin sensitivity to tectonic and climatic forcing: implications of a stochastic model for the role of entrainment and erosion thresholds. Earth Surface Processes and Landforms, **29**: 185–205. John Wiley & Sons, Ltd. doi:[10.1002/ESP.1020](https://doi.org/10.1002/ESP.1020).
- van der Wal, J.L.N., Nottebaum, V.C., Gailleton, B., Stauch, G., Weismüller, C., Batkhishig, O., et al. 2020. Morphotectonics of the northern Bogd fault and implications for Middle Pleistocene to modern uplift rates in southern Mongolia. Geomorphology, **367**: 107330. Elsevier B.V. doi:[10.1016/j.geomorph.2020.107330](https://doi.org/10.1016/j.geomorph.2020.107330).
- Vasudevan, K., Eaton, D.W., and Davidsen, J. 2010. Intraplate seismicity in Canada: a graph theoretic approach to data analysis and interpretation. Nonlinear Processes in Geophysics, **17**: 513–527. doi:[10.5194/npg-17-513-2010](https://doi.org/10.5194/npg-17-513-2010).
- Wahyudi, D.R., Sinclair, H.D., and Mudd, S.M. 2021. Progressive evolution of thrust fold topography in the frontal Himalaya. Geomorphology, **384**: 107717. Elsevier B.V. doi:[10.1016/j.geomorph.2021.107717](https://doi.org/10.1016/j.geomorph.2021.107717).
- Wallach, J., Benn, K., and Rimando, R. 1995. Recent, tectonically induced, surficial stress-relief structures in the Ottawa–Hull area, Canada. Canadian Journal of Earth Sciences, **32**: 325–333. doi:[10.1139/e95-027](https://doi.org/10.1139/e95-027).
- Wang, Y., Zheng, D., Zhang, H., Li, C., Xiao, L., Li, Y., and Hao, Y. 2019. The distribution of active rock uplift in the interior of the western Qilian Shan, NE Tibetan Plateau: inference from bedrock channel profiles. Tectonophysics, **759**: 15–29. Elsevier B.V. doi:[10.1016/j.tecto.2019.04.001](https://doi.org/10.1016/j.tecto.2019.04.001).
- Wheeler, J.O., Hoffman, P.F., Card, K.D., Davidson, A., Sanford, B.V., Okulitch, A.V., and Roest, W.R. 1996. Geological map of Canada. Geological Survey of Canada, “A” Series Map 1860A, 3 sheets; 1 CD-ROM. doi:[10.4095/208175](https://doi.org/10.4095/208175).
- Whipple, K.X., DiBiase, R.A., and Crosby, B.T. 2013. Bedrock rivers. In Treatise on geomorphology. Elsevier Ltd. doi:[10.1016/B978-0-12-374739-6.00254-2](https://doi.org/10.1016/B978-0-12-374739-6.00254-2).
- Wobus, C., Whipple, K.X., Kirby, E., Snyder, N., Johnson, J., Spyropolou, K., et al. 2006. Tectonics from topography: procedures, promise, and pitfalls. Special Paper of the Geological Society of America. Geological Society of America. Vol. **398**, pp. 55–74. doi:[10.1130/2006.2398\(04\)](https://doi.org/10.1130/2006.2398(04)).
- Wolpert, J.A., and Forte, A.M. 2021. Response of transient rock uplift and base level knickpoints to erosional efficiency contrasts in bedrock streams. Earth Surface Processes and Landforms, **462092**. doi:[10.1002/esp.5146](https://doi.org/10.1002/esp.5146).
- Wu, P., and Hasegawa, H.S. 1996. Induced stresses and fault potential in eastern Canada due to a realistic load: a preliminary analysis. Geophysical Journal International, **127**: 215–229. Oxford Academic. doi:[10.1111/j.1365-246X.1996.TB01546.X](https://doi.org/10.1111/j.1365-246X.1996.TB01546.X).
- Xue, L., Alemu, T., Gani, N.D., and Abdelsalam, M.G. 2018. Spatial and temporal variation of tectonic uplift in the southeastern Ethiopian Plateau from morphotectonic analysis. Geomorphology, **309**: 98–111. Elsevier B.V. doi:[10.1016/j.geomorph.2018.02.025](https://doi.org/10.1016/j.geomorph.2018.02.025).
- Yıldırım, C. 2014. Relative tectonic activity assessment of the Tuz Gölü Fault Zone; Central Anatolia, Turkey. Tectonophysics, **630**: 183–192. doi:[10.1016/j.tecto.2014.05.023](https://doi.org/10.1016/j.tecto.2014.05.023).
- Yu, K., Chouinard, L.E., and Rosset, P. 2016. Seismic vulnerability assessment for Montreal. Georisk: Assessment and Management of Risk for Engineered Systems and Geohazards, **10**: 164–178. Taylor & Francis. doi:[10.1080/17499518.2015.1106562](https://doi.org/10.1080/17499518.2015.1106562).